

# Triplet J-driven DNP – a proposal to increase the sensitivity of solution-state NMR without microwave

Maria Grazia Concilio<sup>1\*</sup>, Yiwen Wang<sup>1</sup>, and Linjun Wang<sup>2,3</sup>, Xueqian Kong<sup>1,2\*</sup>

<sup>1</sup>*Institute of Translational Medicine, Shanghai Jiao Tong University, 200240 Shanghai, China*

<sup>2</sup>*Department of Chemistry, Zhejiang University, 310058 Hangzhou, Zhejiang, China*

<sup>3</sup>*Zhejiang Key Laboratory of Excited-State Energy Conversion and Energy Storage, Department of Chemistry, Zhejiang University, 310058 Hangzhou, Zhejiang, China*

## Abstract

Dynamic nuclear polarization (DNP) is an important method to enhance the limited sensitivity of nuclear magnetic resonance (NMR). Using the existing mechanisms such as Overhauser DNP (ODNP) is still difficult to achieve significant enhancement of NMR signals in solutions at a high magnetic field. The recently proposed J-driven DNP (JDNP) condition (when the exchange interaction  $J_{ex}$  of two electron spins matches their Larmor frequency  $\omega_E$ ) may enable signal enhancement in solution as it requires only dipolar interaction between the biradical polarization agent and the analyte. However, likewise ODNP, the current JDNP strategy still requires the saturation of the electron polarization with high microwave power which has poor penetration and is associated with heating effects in most liquids. The replacement of high-power microwave irradiation is possible if the temporal electron polarization imbalance is created by a different wavelength such as the visible light. Here, we propose a triplet-JDNP mechanism which first exploits the light-induced singlet fission process (i.e., a singlet exciton is converted into two triplet excitons). As the JDNP condition  $J_{ex} \approx \pm\omega_E$  is fulfilled, a triplet-to-triplet cross-relaxation process will occur with different rates and consequently lead to the creation of hyperpolarization on the coupled nuclear spin states. This communication discusses the theory behind the triplet-JDNP proposal, as well as the polarizing agents and conditions that will enable the new approach to enhance NMR's sensitivity without the need of microwave irradiation.

**Keywords:** dynamic nuclear polarization, singlet fission, triplet-to-triplet cross relaxation, pentacene dimers

[\\*mariagrazia.concilio@sjtu.edu.cn](mailto:mariagrazia.concilio@sjtu.edu.cn)

[\\*xkong@sjtu.edu.cn](mailto:xkong@sjtu.edu.cn)

## Introduction:

Nuclear Magnetic Resonance (NMR) is one of the most versatile forms of spectroscopy, conveying structure and dynamics information with minimal invasiveness. Further applications of NMR are limited by its poor sensitivity – particularly for liquids at a high magnetic field (7 T – 23 T), where the most analytical applications are performed. Methods based on Overhauser Dynamic Nuclear Polarization (ODNP), [1-4] which transfer polarization from an unpaired electron in a radical polarizing agent to nearby nuclei, can alleviate the sensitivity problem. However, most ODNP approaches applicable today work solely in the presence of scalar electron-nuclear coupling, that arises in a limited number of systems. [5-12] High-field ODNP experiments are usually limited, as they rely on Fermi contact couplings that arise in specific radical/solvent combinations and require an electron delocalization on the target nucleus that occurs only for certain nuclei, such as  $^{31}\text{P}$ , [13, 14]  $^{19}\text{F}$  [5, 15] and  $^{13}\text{C}$ . [6, 7, 12, 16]. For the more general and relevant analytical cases, only intermolecular dipolar hyperfine couplings between  $^1\text{H}$  nuclei and electron radicals are present. [12, 17-19] In these conditions, the ODNP efficiency decays rapidly with the magnetic field,  $B_0$ .

We have recently proposed the J-driven DNP (JDNP) approach to bypass the limitations of high-field ODNP. The JDNP approach relies on the use of a coupled electron spin pair (on a biradical) whose exchange coupling  $J_{\text{ex}}$  matches either the electron or the nuclear Larmor frequency,  $\omega_E$  and  $\omega_N$ , respectively. [20, 21] The physics of the JDNP is reminiscent of that observed in chemically induced dynamic nuclear polarization (CIDNP) [22-25] in which nuclear magnetization enhancement is generated in a spin-correlated radical pair due to a singlet/triplet interconversion process modulated by dipolar hyperfine couplings. In the JDNP, microwaves (rather than the photochemical reactions in CIDNP) are used to drive the system away from the thermal equilibrium. As one of the JDNP conditions (either  $J_{\text{ex}} \approx \pm\omega_E$  or  $J_{\text{ex}} \approx \pm\omega_N$ ) is fulfilled, triplet-to-singlet cross-relaxation rates will occur with different rates for  $\alpha$  and  $\beta$  nuclear spin states, and consequently lead to the creation of longitudinal nuclear polarization. [21]

However, the irradiation of electron spins at their Larmor frequencies (as needed for both ODNP and JDNP) is problematic due to the limited microwave availability, sample heating effects and the low microwave penetration. The photoexcitation process which selects triplet transitions on a fluorescent molecule may also create temporal electron spin polarizations while avoiding the adverse effects of microwave irradiation. Under certain conditions, the electron spin polarization may be transferred to nuclear spins such as in triplet-DNP. [26, 27] However, the current triplet-DNP works in solution only at low magnetic fields ( $<1$  T) and it still needs a microwave source to facilitate the polarization transfer. Bearing in mind the limitations of various DNP techniques (e.g. unfavored microwave irradiation, inaccessible to general liquid samples, etc.), we propose a strategy dubbed triplet-JDNP which utilizes only photoexcitation

to generate spin polarization and should be applicable to general analytes in the liquid state. The triplet-JDNP approach is based upon the singlet fission (SF) process of a triplet-pair system (e.g. on a chromophore dimer) in which a singlet exciton is converted into two triplet excitons by photoexcitation. [28-30] When  $J_{\text{ex}}$  of the two triplets fulfills the JDNP condition  $J_{\text{ex}} \approx \pm \omega_E$ , the population imbalance may be generated on the  $\alpha$  and  $\beta$  nuclear spin states (on the analyte molecule) that are coupled to the triplet pair through dipolar hyperfine interaction.

In a typical four-stage intramolecular SF model (Figure 1), for linked dimers composed by two pentacene chromophores, [31, 32] the absorption of a photon brings one chromophore from its ground state ( $\hat{S}_0$ ) to its lowest-lying excited singlet configuration ( $\hat{S}_1$ ). The resulting photogenerated singlet exciton  $\hat{S}_1\hat{S}_0$  decays into correlated triplet pair states of multiplicity  $M=2S+1$ , where  $S$  is the total spin of the triplet pair state. The state  $\hat{S}_1\hat{S}_0$  (or  $\hat{S}_0\hat{S}_1$ ) corresponds to one pentacene in its first excited state, while the other remains in its ground state. In the case of a symmetric molecule, like the pentacene dimer considered in this study, the state  $\hat{S}_1\hat{S}_0$  is equivalent to the state  $\hat{S}_0\hat{S}_1$ . These states can be labelled as  $^M(\hat{T}\hat{T})_{m_s}$ , where  $m_s$  is the projection of spin angular momentum. In the last stage of the SF, the triplet pair dissociates into two isolated triplets  $\hat{T}_1 + \hat{T}_1$  which later decay away through a recombination process.

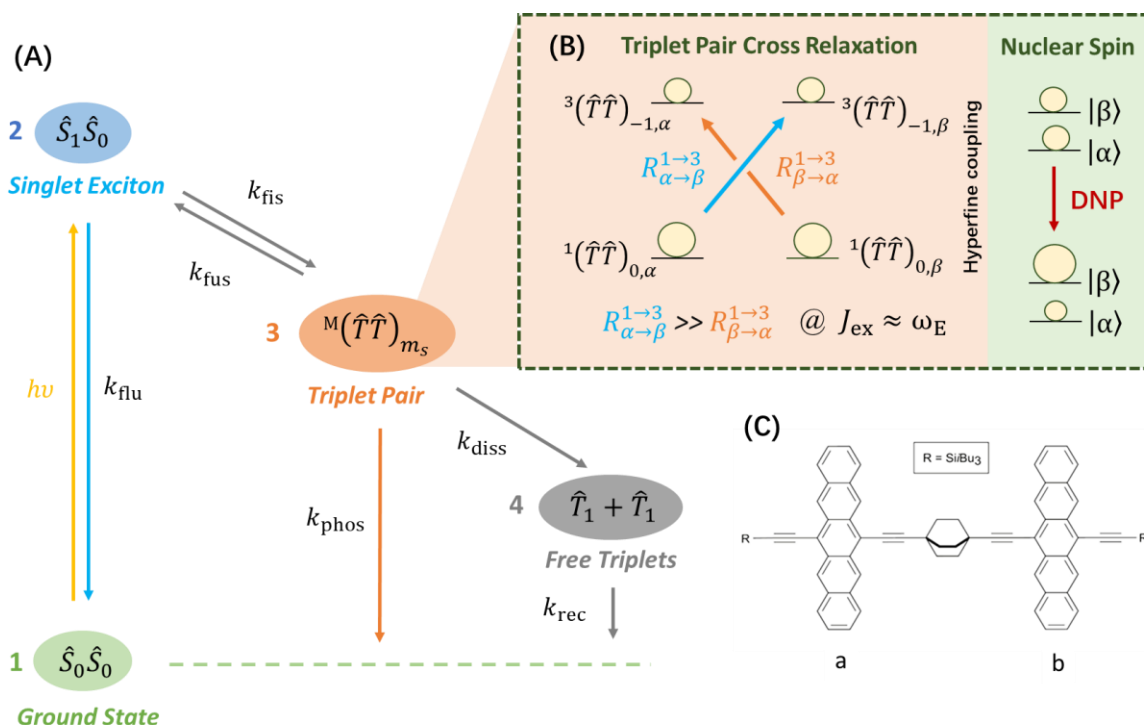


**Figure 1.** (A) The singlet fission scheme, where the constants  $k_{\text{flu}}$ ,  $k_{\text{fis}}$ ,  $k_{\text{fus}}$ ,  $k_{\text{diss}}$ ,  $k_{\text{phos}}$  and  $k_{\text{rec}}$  represent the rates of fluorescence, fission, fusion, dissociation, phosphorescence and recombination respectively. The numbers indicate the

4 stages of the SF process. (B) At the JDNP condition (when  $J_{\text{ex}} \approx \omega_{\text{E}}$  is fulfilled), the triplet-to-triplet cross-relaxation process takes place with different rates from  $^1(\hat{T}\hat{T})_{0,\alpha}$  to  $^3(\hat{T}\hat{T})_{-1,\beta}$  (labeled as  $R_{\alpha \rightarrow \beta}^{1 \rightarrow 3}$ ) and from  $^1(\hat{T}\hat{T})_{0,\beta}$  to  $^3(\hat{T}\hat{T})_{-1,\alpha}$  (labeled as  $R_{\beta \rightarrow \alpha}^{1 \rightarrow 3}$ ). It leads to an increase of the population of the states  $^3(\hat{T}\hat{T})_{-1,\alpha/\beta}$  and creates nuclear spin polarization of coupled protons. (C) The chemical structure of the pentacene dimer considered in this work which is composed of two monomers a and b.

In the case of a coupled triplet pair, there are nine possible spin states that can be constructed and labelled as  $|S, m_s\rangle$ , where  $S$  is equal to 2, 1 and 0. Five states with  $S = 2$  and  $M = 5$  are termed as  $^5(\hat{T}\hat{T})_{0,\pm 1,\pm 2}$ , three states with  $S = 1$  and  $M = 3$  are termed as  $^3(\hat{T}\hat{T})_{0,\pm 1}$ , and one state with  $S = 0$  and  $M = 1$  is termed as  $^1(\hat{T}\hat{T})_0$ . The initial triplet pair formed by SF has overall singlet character and corresponds to the state  $^1(\hat{T}\hat{T})_0$ . Subsequently, the states  $^3(\hat{T}\hat{T})_{0,\pm 1}$  and  $^5(\hat{T}\hat{T})_{0,\pm 1,\pm 2}$  are populated through relaxation or intersystem crossing (ISC). [31] For the analysis of JDNP condition, triplet pair states are coupled to nuclear spins (represented by a proton with  $\alpha$  and  $\beta$  spin states) through dipolar hyperfine interaction. As  $J_{\text{ex}} \approx \pm\omega_{\text{E}}$  is fulfilled at the JDNP condition, a population imbalance between the  $\alpha$  and  $\beta$  nuclear components of the triplet pair states takes place (represented as  $^1(\hat{T}\hat{T})_{0,\alpha/\beta}$ ,  $^3(\hat{T}\hat{T})_{0,\pm 1,\alpha/\beta}$  and  $^5(\hat{T}\hat{T})_{0,\pm 1,\pm 2,\alpha/\beta}$ ) and hence hyperpolarization is created on the coupled protons. Nuclear polarization arises in particular from the states  $^1(\hat{T}\hat{T})_{0,\alpha/\beta}$  and  $^3(\hat{T}\hat{T})_{\pm 1,\alpha/\beta}$  (specifically  $^3(\hat{T}\hat{T})_{-1,\alpha/\beta}$  in the case of positive  $J_{\text{ex}}$  and  $^3(\hat{T}\hat{T})_{+1,\alpha/\beta}$  in the case of negative  $J_{\text{ex}}$ ). In this communication, we describe the mechanisms of triplet-JDNP using the Redfield theory [33] and also discuss the potential polarizing agents and conditions for enhancement optimization.

### Spin system and simulation methodology:

A non-conjugated pentacene dimer with structure shown in Figure 1 was considered as the model system in this work. [31, 32] The singlet fission process involves states corresponding to the singlet ground state, the singlet exciton, the triplet pair states and the isolated triplet states. The dynamics of these excited states is usually modelled with either the Lindblad or the Bloch-Redfield master equation. [34] However, these formalisms do not support relaxation arising from tensor anisotropies from which the triplet-JDNP arises. Therefore, we used the Liouville space formulation of Bloch-Redfield-Wangsness (BRW) relaxation theory. [35, 36] Within the BRW formalism, it is not possible to create basis sets that describe the electronic states simultaneously in the same spin space. In addition, the triplet-JDNP effect arises only from the triplet pair states coupled to nuclear spin states. Therefore, our time domain simulations were performed using an approach similar to the one used to simulate the magnetic field effects in photoluminescence and CIDNP. [37, 38] We built a spin system composed by a triplet pair with two spin-1 and one proton spin-1/2 that interact solely through anisotropic dipolar hyperfine couplings (scalar

hyperfine couplings were not included). As in JDNP, we observed a constant and spherical symmetric distribution of the enhancement in the region surrounding the triplet-dimer. [20] A proton can get polarized in a distance from 0.5 Å up to 5 Å away from each monomer. Therefore, in our simulations, distances between the two triplets (belonging to the radical) and the proton (belonging to an assumed solvent molecule) were set to 3 Å and 17 Å respectively (the actual proton and triplet Cartesian coordinates are reported in Table 1), that corresponds to a proton in the region 0.5 Å - 5 Å away from each monomer. In order to simulate the SF process, we used a system of four coupled Liouville von Neumann equations to describe the time evolution of different states (see Eq. (3) later). In the numerical implementation, the Liouvillian is a supermatrix and the initial condition corresponds to a state vector containing the states  $\hat{S}_0\hat{S}_0$ ,  $\hat{S}_1\hat{S}_0$ ,  $^M(\hat{T}\hat{T})_{m_s}$  and  $\hat{T}_1 + \hat{T}_1$ . The electron  $g$ -tensors were set with the eigenvalues taken from those found in pentacene in a single crystal of naphthalene, [39, 40] and the zero field splitting parameters D and E were set equal to 1139 MHz and 60 MHz as those observed in pentacene dimers. [41, 42] The rotational correlation time of the biradical/proton dipolar hyperfine coupled triad was set to 300 ps, as it should be longer than the rotational correlation time determined for the TIPS-pentacene. [43] Numerical simulations took into account of all self- and cross-relaxation terms within the BRW relaxation theory, [33, 36] and considered the local vibrational relaxation modes arising from the mixing between spin and orbital angular momentum (which often dominates the electron relaxation rates of organic radicals). [43] Spectral density functions describing the relaxation rates were computed with the pattern matching algorithm. [36] The kinetics constants  $k_{flu}$ ,  $k_{fis}$ ,  $k_{fus}$ ,  $k_{diss}$ ,  $k_{phos}$  and  $k_{rec}$  involved in the SF model shown in Figure 1 were determined experimentally using transient absorption spectroscopy and were taken from ref. [31]. All the simulation parameters are summarized in Table 1. Time domain simulations were performed with the Spinach software. [44]

**Table 1:** Parameters for the triplet-pair / proton spin system used in the simulations.

Parameter	Value
$^1\text{H}$ chemical shift tensor, ppm	[5 5 5]
Triplet 1 $g$ -tensor eigenvalues, [xx yy zz] / Bohr magneton*	[2.0015 2.0009 2.0005]
Triplet 1 $g$ -tensor, ZYZ active Euler angles / rad	[0.0 0.0 0.0]
Triplet 2 $g$ -tensor eigenvalues, [xx yy zz] / Bohr magneton*	[2.0015 2.0009 2.0005]
Triplet 2 $g$ -tensor, ZYZ active Euler angles / rad	[0.0 0.0 0.0]
Zero field splitting, D / MHz and E / MHz	1139 and 60
$^1\text{H}$ coordinates [x y z] / Å	[0 0 0 10]
Triplet 1 and triplet 2 coordinates, [x y z] / Å	[0 0 -7] and [0 0 7]

Rotational correlation time $\tau_C$ / ps	300
Kinetics constants, $k_{\text{flu}}$ , $k_{\text{fis}}$ , $k_{\text{fus}}$ , $k_{\text{phos}}$ , $k_{\text{diss}}$ and $k_{\text{rec}}$ / s <sup>-1</sup>	$9.5 \times 10^7$ , $2.4 \times 10^9$ , $5 \times 10^7$ , $1 \times 10^7$ , $5.7 \times 10^6$ , $3 \times 10^4$
Local mode relaxation / Hz	$1 \times 10^4$
Temperature / K	298

\*Simulations used Zeeman interaction tensors that were made axially symmetric along the main molecular axis (corresponding for instance, to a linker connecting two pentacene units).

The nine triplet pair states can be represented in terms of the two spin-1 bases [45]:

$$\begin{aligned}
{}^5(\hat{T}\hat{T})_{\pm 2} &= |\hat{T}_{\pm}\hat{T}_{\pm}\rangle, \quad {}^5(\hat{T}\hat{T})_{\pm 1} = \frac{|\hat{T}_0\hat{T}_{\pm}\rangle + |\hat{T}_{\pm}\hat{T}_0\rangle}{\sqrt{2}}, \quad {}^5(\hat{T}\hat{T})_0 = \frac{|\hat{T}_-\hat{T}_+\rangle + 2|\hat{T}_0\hat{T}_0\rangle + |\hat{T}_+\hat{T}_-\rangle}{\sqrt{6}}, \\
{}^3(\hat{T}\hat{T})_{\pm 1} &= \frac{|\hat{T}_0\hat{T}_{\pm}\rangle - |\hat{T}_{\pm}\hat{T}_0\rangle}{\sqrt{2}}, \quad {}^3(\hat{T}\hat{T})_0 = \frac{|\hat{T}_+\hat{T}_-\rangle - |\hat{T}_-\hat{T}_+\rangle}{\sqrt{2}} \\
{}^1(\hat{T}\hat{T})_0 &= \frac{|\hat{T}_-\hat{T}_+\rangle - |\hat{T}_0\hat{T}_0\rangle + |\hat{T}_+\hat{T}_-\rangle}{\sqrt{3}}
\end{aligned} \tag{1}$$

The triplet pair states combined with the proton spin states  $\alpha$  and  $\beta$  correspond to:

$$\begin{aligned}
{}^5(\hat{T}\hat{T})_{\pm 2, \alpha/\beta} &= |\hat{T}_{\pm}\hat{T}_{\pm}\alpha/\beta\rangle, \quad {}^5(\hat{T}\hat{T})_{\pm 1, \alpha/\beta} = \frac{|\hat{T}_0\hat{T}_{\pm}\alpha/\beta\rangle + |\hat{T}_{\pm}\hat{T}_0\alpha/\beta\rangle}{\sqrt{2}}, \quad {}^5(\hat{T}\hat{T})_{0, \alpha/\beta} = \frac{|\hat{T}_-\hat{T}_+\alpha/\beta\rangle + 2|\hat{T}_0\hat{T}_0\alpha/\beta\rangle + |\hat{T}_+\hat{T}_-\alpha/\beta\rangle}{\sqrt{6}} \\
{}^3(\hat{T}\hat{T})_{\pm 1, \alpha/\beta} &= \frac{|\hat{T}_0\hat{T}_{\pm}\alpha/\beta\rangle - |\hat{T}_{\pm}\hat{T}_0\alpha/\beta\rangle}{\sqrt{2}}, \quad {}^3(\hat{T}\hat{T})_{0, \alpha/\beta} = \frac{|\hat{T}_+\hat{T}_-\alpha/\beta\rangle - |\hat{T}_-\hat{T}_+\alpha/\beta\rangle}{\sqrt{2}} \\
{}^1(\hat{T}\hat{T})_{0, \alpha/\beta} &= \frac{|\hat{T}_-\hat{T}_+\alpha/\beta\rangle - |\hat{T}_0\hat{T}_0\alpha/\beta\rangle + |\hat{T}_+\hat{T}_-\alpha/\beta\rangle}{\sqrt{3}}
\end{aligned} \tag{2}$$

Triplet pair states are constructed with the Clebsch-Gordon coefficients in the Hilbert space [46] and irreducible spherical tensor operator (ISTO) are used in the time domain Liouville space simulations. In the later context, the state symbols are also used to indicate the corresponding state amplitude. ISTO of the states given in Eqs. 1 and 2 were determined with the software SpinDynamica (<https://www.spindynamica.soton.ac.uk/>) and were then implemented into the software Spinach [44]. The SF process shown in Figure 1 can be represented with a set of coupled Liouville von Neumann equations:

$$\begin{aligned}
\frac{\partial \hat{\rho}_1(t)}{\partial t} &= k_{\text{flu}} \hat{\rho}_2(t) + k_{\text{phos}} \hat{\rho}_3(t) + k_{\text{rec}} \hat{\rho}_4(t) \\
\frac{\partial \hat{\rho}_2(t)}{\partial t} &= -(k_{\text{flu}} + k_{\text{fis}}) \hat{\rho}_2(t) + k_{\text{fus}} {}^1(\hat{T}\hat{T})_{0,L} \hat{\rho}_3(t) {}^1(\hat{T}\hat{T})_{0,R} \\
\frac{\partial \hat{\rho}_3(t)}{\partial t} &= k_{\text{fis}} \hat{\rho}_2(t) - i \left[ \hat{L}, \hat{\rho}_3(t) \right] - \frac{k_{\text{fus}}}{2} \left[ {}^1(\hat{T}\hat{T})_0, \hat{\rho}_3(t) \right]_+ - (k_{\text{diss}} + k_{\text{phos}}) \hat{\rho}_3(t)
\end{aligned} \tag{3}$$

$$\frac{\partial \hat{\rho}_4(t)}{\partial t} = k_{\text{diss}} \hat{\rho}_3(t) - k_{\text{rec}} \hat{\rho}_4(t)$$

where  $\hat{\rho}_{1-4}(t)$  correspond to the states  $\hat{S}_0\hat{S}_0$ ,  $\hat{S}_1\hat{S}_0$ ,  ${}^M(\hat{T}\hat{T})_{ms} = {}^M(\hat{T}\hat{T})_{ms/\alpha} + {}^M(\hat{T}\hat{T})_{ms/\beta}$  and  $\hat{T}_1 + \hat{T}_1$  respectively;  ${}^1(\hat{T}\hat{T})_{0,L}$  and  ${}^1(\hat{T}\hat{T})_{0,R}$  are the left- and right-side product superoperators of the state  ${}^1(\hat{T}\hat{T})_0$ ;  $[{}^1(\hat{T}\hat{T})_0, \hat{\rho}_3(t)]_+ = {}^1(\hat{T}\hat{T})_{0,L}\hat{\rho}_3(t) + \hat{\rho}_3(t){}^1(\hat{T}\hat{T})_{0,R}$  is the anticommutation superoperator;  $\hat{L}$  is the Liouvillian superoperator. Eq. (3) can be numerically implemented by building a joint Liouville space of the four sites, all the operators were built considering a spin system composed by two spin-1 and one proton spin-1/2. The Liouvillian superoperator becomes a supermatrix equal to:

$$\hat{L} = \hat{H} + \hat{R} + \hat{K} \quad (4)$$

where  $\hat{H}$ ,  $\hat{R}$  and  $\hat{K}$  are the spin Hamiltonian supermatrix, the relaxation supermatrix and the kinetics supermatrix, respectively. They correspond to:

$$\hat{H} = \begin{pmatrix} \hat{0} & \hat{0} & \hat{0} & \hat{0} \\ \hat{0} & \hat{0} & \hat{0} & \hat{0} \\ \hat{0} & \hat{0} & \hat{H}_{\text{TT}} & \hat{0} \\ \hat{0} & \hat{0} & \hat{0} & \hat{0} \end{pmatrix}, \hat{R} = \begin{pmatrix} \hat{0} & \hat{0} & \hat{0} & \hat{0} \\ \hat{0} & \hat{0} & \hat{0} & \hat{0} \\ \hat{0} & \hat{0} & \hat{R}_{\text{TT}} & \hat{0} \\ \hat{0} & \hat{0} & \hat{0} & \hat{0} \end{pmatrix},$$

$$\hat{K} = \begin{pmatrix} \hat{0} & k_{\text{flu}}\hat{1} & k_{\text{phos}}\hat{1} & k_{\text{rec}}\hat{1} \\ \hat{0} & -(k_{\text{flu}} + k_{\text{fis}})\hat{1} & k_{\text{fus}}[{}^1(\hat{T}\hat{T})_L \cdot {}^1(\hat{T}\hat{T})_R] & \hat{0} \\ \hat{0} & k_{\text{fis}}\hat{1} & \frac{k_{\text{fus}}}{2}[{}^1(\hat{T}\hat{T})_L + {}^1(\hat{T}\hat{T})_R] - (k_{\text{diss}} + k_{\text{phos}})\hat{1} & \hat{0} \\ \hat{0} & \hat{0} & k_{\text{diss}}\hat{1} & -k_{\text{rec}}\hat{1} \end{pmatrix} \quad (5)$$

where  $\hat{H}_{\text{TT}}$  is the laboratory frame spin Hamiltonian that contains all the interactions present in the coupled spin system of the triplet pair and the proton, while  $\hat{R}_{\text{TT}}$  is the relaxation superoperator that contains all the relaxation mechanisms arising from tensor anisotropies and relaxation from local vibrational modes.  $\hat{0} = \begin{pmatrix} 0 & \dots & 0 \\ \vdots & \ddots & \vdots \\ 0 & \dots & 0 \end{pmatrix}$  and  $\hat{1} = \begin{pmatrix} 1 & \dots & 0 \\ \vdots & \ddots & \vdots \\ 0 & \dots & 1 \end{pmatrix}$  are the zero and the unit matrices respectively with the same dimension of  $\hat{H}_{\text{TT}}$  and  $\hat{R}_{\text{TT}}$ . The laboratory frame Hamiltonian corresponds to:

$$\begin{aligned} \hat{H} &= \hat{H}_{Z,a} + \hat{H}_{Z,b} + \hat{H}_{Z,N} + \hat{H}_{ZFS,a} + \hat{H}_{ZFS,b} + \hat{H}_{DD} + \hat{H}_J + \hat{H}_{HF} \\ &= \sum_{k=a,b} \hat{S}^{(k)} \cdot \mathbf{G}_E^{(k)} \cdot \hat{\mathbf{B}}_0 + \hat{\mathbf{N}} \cdot \mathbf{G}_N \cdot \hat{\mathbf{B}}_0 + \sum_{k=a,b} \hat{S}^{(k)} \cdot \mathbf{Z}^{(k)} \cdot \hat{S}^{(k)} + \\ &\quad \hat{S}^{(a)} \cdot (\mathbf{D} + J_{\text{ex}}) \cdot \hat{S}^{(b)} + \sum_{k=a,b} \hat{S}^{(k)} \cdot \mathbf{A}^{(k)} \cdot \hat{\mathbf{N}} \end{aligned} \quad (6)$$

where  $\widehat{H}_{Z,a}$ ,  $\widehat{H}_{Z,b}$  and  $\widehat{H}_{Z,N}$  represent the Zeemann interaction of the triplets in the monomers a and b and of the nuclear spin respectively,  $\widehat{H}_{ZFS,a}$  and  $\widehat{H}_{ZFS,b}$  represent the ZFS interaction of the triplet in the two monomers a and b respectively,  $\widehat{H}_{DD}$  represents the inter-electron dipolar interaction,  $\widehat{H}_J$  represents the inter-electron exchange coupling and  $\widehat{H}_{HF}^{(k)}$  represents the dipolar hyperfine interaction.  $\widehat{S}^{(k)}$  with  $k = a$  and  $b$  is a vector with the electron spin operators for the triplets in monomers a and b,  $\widehat{N}$  is a vector with the nuclear spin operators,  $\widehat{B}_0$  is the magnetic field vector,  $\mathbf{G}_E^{(k)}$  and  $\mathbf{Z}^{(k)}$  are the electron Zeeman and ZFS interaction tensors,  $\mathbf{G}_N$  is the nuclear Zeeman interaction tensor,  $\mathbf{D}$  is the inter-electron dipolar interaction tensor and  $\mathbf{A}^{(k)}$  is the dipolar hyperfine interaction tensor between the nucleus and the indicated electron  $k$ . The Redfield relaxation superoperator and the analytical expressions of the cross- and self-relaxation rates involving two states a and b were computed in according to:

$$\left\langle \widehat{\rho}_a \left| \widehat{R}_{ab} \right| \widehat{\rho}_b \right\rangle = \sum_{kmpq} \int_0^\infty G_{kmpq}(\tau) \text{Tr} \left( \widehat{\rho}_a^\dagger \left[ \widehat{Q}_{km}, \left[ e^{i\widehat{H}_0\tau} \widehat{Q}_{pq}^\dagger e^{-i\widehat{H}_0\tau}, \widehat{\rho}_b \right] \right] \right) d\tau \quad (7)$$

where  $\widehat{R}_{ab}$  is the relaxation superoperator,  $G_{kmpq}(\tau)$  is the correlation function between two Wigner functions that perform the ensemble average [36];  $\widehat{H}_0$  is the static part of the Hamiltonian;  $\widehat{Q}_{km(pq)}$  are the rotational basis operators of the anisotropic part of the Hamiltonian. [33, 36] Time domain simulations were performed using the Liouville von Neumann equation of motion:

$$\frac{\partial \widehat{\rho}(t)}{\partial t} = \widehat{\rho}(0) \exp(-\widehat{L}t) \quad (8)$$

where  $\widehat{\rho}(0) = [\widehat{\rho}_1(0), \widehat{\rho}_2(0), \widehat{\rho}_3(0), \widehat{\rho}_4(0)]$  and  $\widehat{\rho}(t) = [\widehat{\rho}_1(t), \widehat{\rho}_2(t), \widehat{\rho}_3(t), \widehat{\rho}_4(t)]$  are supervectors containing the state vectors of four species involved in the SF at the time zero and at the time  $t$  respectively. Simulations were performed by setting the initial condition to  $\widehat{\rho}(0)=[0,1,0,0]$ , corresponding to the  $\widehat{S}_1\widehat{S}_0$  state being fully populated, while the populations of the other states were set to zero. The  $\widehat{S}_1\widehat{S}_0$  state was set equal to  ${}^1(\widehat{T}\widehat{T})_0$  representing the triplet states with singlet character, in the simulations of the SF process, it is moved in the triplet pair subspace of the joint Liouville space in according to the  $k_{fis}$  and  $k_{fus}$  rates due to the  ${}^1(\widehat{T}\widehat{T})_{0,L}$  and  ${}^1(\widehat{T}\widehat{T})_{0,R}$  operators in Eq. 3. Time evolution of the observable operator  $\widehat{O}$ , corresponding to the population of triplet pair states, was calculated by taking their scalar products with the state vector  $\widehat{\rho}_n(t)$ , with  $n=1-4$  (corresponding to the vectors in Eq. (3)), at each time step:

$$\widehat{O}(t) = \langle \widehat{O} | \widehat{\rho}_n(t) \rangle \quad (9)$$

The time dynamics of  $\hat{S}_0\hat{S}_0(t)$ ,  $\hat{S}_1\hat{S}_0(t)$  and  $\hat{T}_1 + \hat{T}_1(t)$  was computed by summing the amplitude of all the triplet pair states  ${}^M(\hat{T}\hat{T})_{ms,\alpha/\beta}$ , computed in according Eq. (9), using the vectors  $\hat{\rho}_1(t)$ ,  $\hat{\rho}_2(t)$  and  $\hat{\rho}_4(t)$  in Eq. (3). In our kinetics model we did not take into account of the correlated singlet–triplet pair states, since they were not observed in the time-resolved electron paramagnetic resonance (TREPR) spectrum of the molecule under consideration. [31, 32] Singlet–triplet pair states are expected to arise in molecules where heavy atoms are present. [47] Simulations were performed from 0 T to 14.1 T. The evolution of  $k_{\text{fis}}$  and  $k_{\text{fus}}$  with the magnetic field can be predicted with the Merrifield model. [46, 48, 49] According to the Merrifield model, the kinetics constants  $k_{\text{fis}} = k_{\text{fis}} |C_{\text{singlet}}^l|^2$  and  $k_{\text{fus}} = k_{\text{fus}} |C_{\text{singlet}}^l|^2$  are dependent on the magnetic field due to the dependence of the singlet character  $C_{\text{singlet}}^l = \langle {}^1(\hat{T}\hat{T})_0 | \varphi_l \rangle$  where  $\varphi_l$  with  $l = 1-9$  are the eigenstates of the spin Hamiltonian of the triplet pair at a given the magnetic field. [49]  $C_{\text{singlet}}^l$  represents the amount of  ${}^1(\hat{T}\hat{T})_0$  in the eigenstates. In solids, the anisotropic parts of the spin interactions lead to variations of  $C_{\text{singlet}}^l$  with the magnetic field, but in liquids they are averaged out. Therefore,  $C_{\text{singlet}}^l$  is set to 1 at the magnetic fields considered in this work, and consequently the SF kinetic rates are expected to remain constant with the magnetic field (see Figure S1 in the supporting material for more details).

## Results and discussion:

### The photo-kinetics of Triplet-JDNP:

The inter-electron exchange coupling  $J_{\text{ex}}$  of the pentacene dimer shown in Figure 1 is about 15 GHz. This value was used to simulate the TREPR experiments on pentacene dimers. [42] Therefore, we performed triplet-JDNP simulations at 0.55 T to fulfill the JDNP condition  $J_{\text{ex}} \approx \omega_E = 15$  GHz. The simulation results are shown in Figure 2.

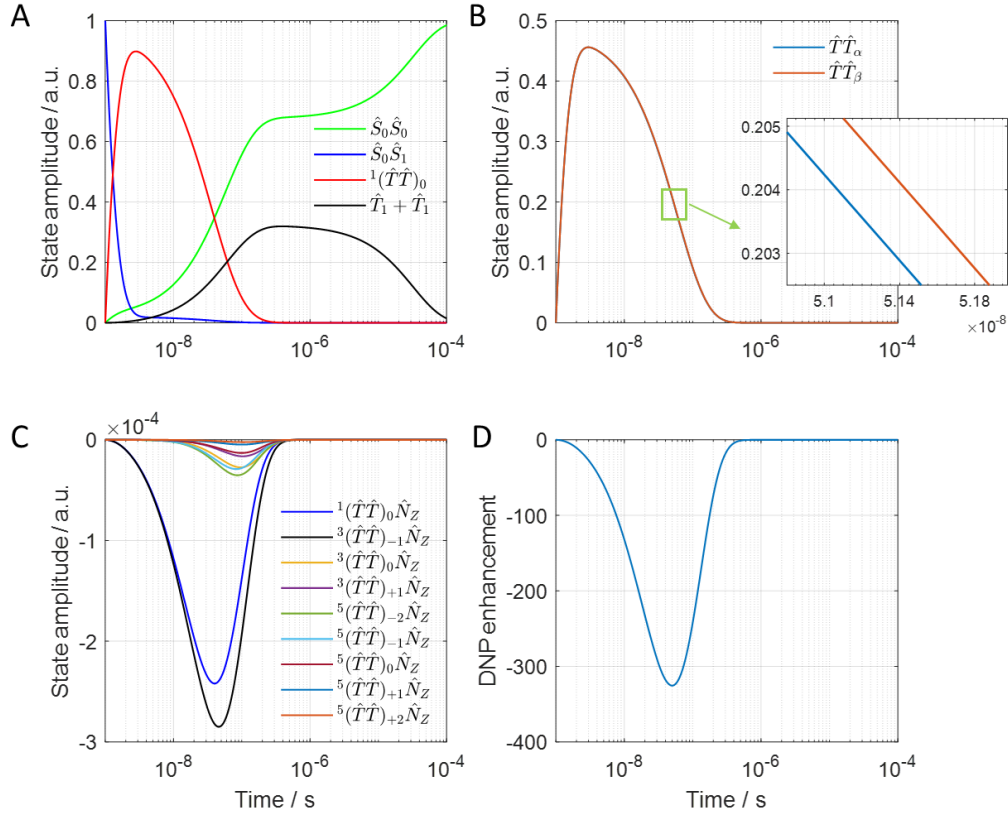


**Figure 2.** (A) Time domain simulations performed at 0.55 T, showing the evolution of the singlet ground state, singlet exciton, the triplet pair state with singlet character and the dissociated triplet states. (B) The sum of the  $\alpha$  and  $\beta$  nuclear components of the nine triplet pair states, indicated as  $\hat{T}\hat{T}_\alpha$  and  $\hat{T}\hat{T}_\beta$ . (C) States arising from the imbalance between the  $\alpha$  and  $\beta$  components of the triplet pair states, indicated with the states  ${}^M(\hat{T}\hat{T})_{m_s}\hat{N}_Z$ , where  $\hat{N}_Z$  represents the nuclear magnetization. (D)  ${}^1\text{H}$  DNP enhancement at different time points. The DNP enhancement represents the achieved nuclear polarization, normalized by its Boltzmann counterpart at the same temperature and field. The other simulation parameters are given in Table 1.

The time evolution of the states shown in Figure 2A is consistent with that observed experimentally using transient optical absorption spectroscopy. [31, 32] At thermal equilibrium, the pentacene dimer exists in its singlet ground state, represented by the state  $\hat{S}_0\hat{S}_0$ . There is a negligible difference between the populations of the  $\alpha$  and  $\beta$  nuclear states, Figure 2B. After the laser irradiation, the singlet exciton  $\hat{S}_1\hat{S}_0$  is created (set as time zero in our simulations). Afterwards, the singlet exciton is converted to the state  ${}^1(\hat{T}\hat{T})_0$  with a fission rate  $k_{\text{fis}}$ . The states  ${}^3(\hat{T}\hat{T})_{0,\pm 1}$  and  ${}^5(\hat{T}\hat{T})_{0,\pm 1,\pm 2}$  are then populated due to the relaxation mechanisms described by the relaxation superoperator. Subsequently, the triplet pair states dissociate into free triplets  $\hat{T}_1 + \hat{T}_1$  (which do not contribute to nuclear polarization under the JDNP mechanism), and

eventually decay to the ground states  $\hat{S}_0\hat{S}_0$ . The lifetimes of  $\hat{S}_1\hat{S}_0$ , the triplet pair states and the dissociated triplets are about 0.004  $\mu\text{s}$ , 0.4  $\mu\text{s}$  and 99  $\mu\text{s}$  respectively. The triplet pair states are coupled to the nuclear spin states  $\alpha$  and  $\beta$  (indicated as  $^M(\hat{T}\hat{T})_{m_s, \alpha/\beta}$ ). The time evolution of the sum of  $\alpha$  and  $\beta$  nuclear components of the nine triplet pair states, represented as  $\hat{T}\hat{T}_\alpha$  and  $\hat{T}\hat{T}_\beta$ , is shown in Figure 2B. As the JDNP condition is fulfilled, [20, 21] a population imbalance between  $^M(\hat{T}\hat{T})_{m_s/\alpha}$  and  $^M(\hat{T}\hat{T})_{m_s/\beta}$  states takes place, populating the states  $^M(\hat{T}\hat{T})_{m_s} \hat{N}_Z$  (Figure 2C). The nuclear polarization is created from the population difference between the states  $\hat{T}\hat{T}_\alpha$  and  $\hat{T}\hat{T}_\beta$  in according to the relation:

$$\hat{N}_Z = \hat{T}\hat{T}_\alpha - \hat{T}\hat{T}_\beta \quad (10)$$

where:

$$\hat{T}\hat{T}_{\alpha/\beta} = \frac{{}^1(\hat{T}\hat{T})_{0,\alpha/\beta} + {}^3(\hat{T}\hat{T})_{0,\alpha/\beta} + {}^3(\hat{T}\hat{T})_{\pm 1,\alpha/\beta} + {}^5(\hat{T}\hat{T})_{0,\alpha/\beta} + {}^5(\hat{T}\hat{T})_{\pm 1,\alpha/\beta} + {}^5(\hat{T}\hat{T})_{\pm 1,\alpha/\beta} + {}^5(\hat{T}\hat{T})_{\pm 2,\alpha/\beta}}{2} \quad (11)$$

The build-up of the nuclear polarization is a transient event that lasts about 0.5  $\mu\text{s}$  and reaches its maximum 0.05  $\mu\text{s}$  after the laser irradiation (see Figure 2D). In the case of positive  $J_{\text{ex}}$ , the nuclear polarization arises mostly from an imbalance between the  $\alpha$  and  $\beta$  nuclear components of the  ${}^1(\hat{T}\hat{T})_0$  and  ${}^3(\hat{T}\hat{T})_{-1}$  states. In the case of negative  $J_{\text{ex}}$ , the state  ${}^3(\hat{T}\hat{T})_{+1}$  is involved instead of the state  ${}^3(\hat{T}\hat{T})_{-1}$ . The ‘‘polarization region’’ in which the triplet JDNP is active is when the electron-nuclear distances are within 5  $\text{\AA}$ . In an actual experiment, the solvent proton diffuses randomly at  $\approx 10 \text{ \AA}/\mu\text{s}$  (*i.e.* 0.001  $\mu\text{m}/\mu\text{s}$  with a diffusion constant of  $10^{-12} \text{ m}^2 \text{ ms}^{-1}$  at 25  $^\circ\text{C}$ ), [17] crossing several times in-and-out of the ‘‘polarization region’’. Considering a solvent proton located at 3  $\text{\AA}$  away from one of the triplets, it will take about 0.2  $\mu\text{s}$  to become sufficiently polarized and then move out of the ‘‘polarization region’’ into the bulk where the nuclear relaxation is longer. As such, the polarization of the proton is enhanced and preserved.

### The polarization mechanism behind the triplet-JDNP:

As the JDNP condition is fulfilled, the energies of the states, including  ${}^1(\hat{T}\hat{T})_0$  and  ${}^3(\hat{T}\hat{T})_{-1}$ ,  ${}^3(\hat{T}\hat{T})_0$  and  ${}^5(\hat{T}\hat{T})_{-2}$ , as well as  ${}^3(\hat{T}\hat{T})_{+1}$  and  ${}^5(\hat{T}\hat{T})_{-1}$ , cross with each other respectively at 0.55 T (Figure 3A). We observed a difference in the triplet-to-triplet cross-relaxation rates between the states  ${}^1(\hat{T}\hat{T})_{0,\alpha} \rightarrow {}^3(\hat{T}\hat{T})_{-1,\beta}$  and  ${}^1(\hat{T}\hat{T})_{0,\beta} \rightarrow {}^3(\hat{T}\hat{T})_{-1,\alpha}$  (Figure 3B) according to the Redfield theory [36].

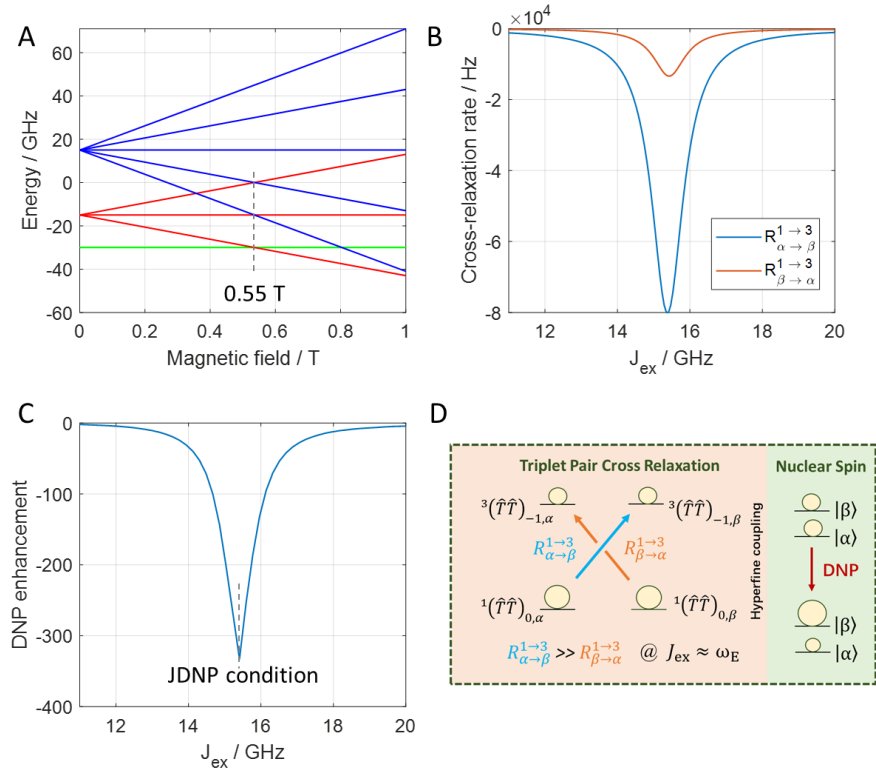


**Figure 3.** (A) Energy level diagram of the triplet pair states at different magnetic fields. The green line corresponds to the state  $^1(\hat{T}\hat{T})_0$ , the red lines correspond to the three states  $^3(\hat{T}\hat{T})_{0,\pm 1}$  and the blue lines correspond to the five states  $^5(\hat{T}\hat{T})_{0,\pm 1,\pm 2}$ . The dashed line indicates the level-crossing of energy levels at 0.55 T. (B) Triplet-to-triplet cross-relaxation rates  $R_{\alpha \rightarrow \beta}^{1 \rightarrow 3}$  and  $R_{\beta \rightarrow \alpha}^{1 \rightarrow 3}$ , as functions of  $J_{\text{ex}}$ . (C)  $^1\text{H}$  DNP enhancement obtained as a function of  $J_{\text{ex}}$ . (D) Diagram showing the states that cross-relax to each other with rates  $R_{\alpha \rightarrow \beta}^{1 \rightarrow 3}$  and  $R_{\beta \rightarrow \alpha}^{1 \rightarrow 3}$ , leading to nuclear polarization  $\hat{N}_Z$ . The simulation parameters are given in Table 1.

The cross-relaxation rates between states  $^1(\hat{T}\hat{T})_{0,\alpha/\beta}$  and  $^3(\hat{T}\hat{T})_{-1,\beta/\alpha}$  can be described by the spectral density functions:  $R_{\alpha \rightarrow \beta}^{1 \rightarrow 3} = \frac{4}{45} \Delta_{\text{HFC}_1 - \text{HFC}_2}^2 J(J_{\text{ex}} + \omega_E + \omega_N)$  for  $^1(\hat{T}\hat{T})_{0,\alpha} \rightarrow ^3(\hat{T}\hat{T})_{-1,\beta}$  (12)

and:

$$R_{\beta \rightarrow \alpha}^{1 \rightarrow 3} = \frac{2}{135} \Delta_{\text{HFC}_1 - \text{HFC}_2}^2 J(J_{\text{ex}} + \omega_E - \omega_N) \text{ for } ^1(\hat{T}\hat{T})_{0,\beta} \rightarrow ^3(\hat{T}\hat{T})_{-1,\alpha} \quad (13)$$

where the term  $\Delta_{\text{HFC}_1 - \text{HFC}_2}^2$  is the a second rank norm squared [50] arising from the difference of the anisotropy of the two dipolar hyperfine coupling tensor matrices, indicated with  $\text{HFC}_1$  and  $\text{HFC}_2$ .  $J(\omega)$  is the spectral density function at a frequency  $\omega$  corresponding to  $\tau_C / (1 + \tau_C^2 \omega^2)$  arising from the Fourier

transform of the correlation function in Eq. 7,[33, 36] where  $\tau_C$  is the rotational correlation time. The difference between the two dipolar hyperfine tensor anisotropies creates a cross-relaxation path between the states  $^1(\hat{T}\hat{T})_{0,\alpha/\beta}$  and  $^3(\hat{T}\hat{T})_{-1,\beta/\alpha}$ . Tensor anisotropies do not create cross-relaxation paths between  $^3(\hat{T}\hat{T})_{0,\alpha/\beta}$  and  $^5(\hat{T}\hat{T})_{-2,\beta/\alpha}$ , or between  $^3(\hat{T}\hat{T})_{+1,\alpha/\beta}$  and  $^5(\hat{T}\hat{T})_{-1,\beta/\alpha}$ . The difference between the cross-relaxation rates  $\Delta R_{\text{cross}} = R_{\alpha \rightarrow \beta}^{1 \rightarrow 3} - R_{\beta \rightarrow \alpha}^{1 \rightarrow 3} \neq 0$  arises due to the presence of different denominators of the spectral density functions describing the rates.  $\Delta R_{\text{cross}}$  leads to an imbalance between the  $\alpha$  and  $\beta$  nuclear spin states and consequently to the DNP enhancement (Figure 3C), in according to the polarization mechanism shown in Figure 3D. We also analyzed the self-relaxation rates  $R^{[M\hat{T}\hat{T}_{m_s,\alpha}]}$  and  $R^{[M\hat{T}\hat{T}_{m_s,\beta}]}$  which arise due to tensor anisotropies (see supporting material for more details). The results showed that the self-relaxation rates do not contribute directly to the DNP enhancement but indirectly to increase the populations of the triplet pair states from the state  $^1(\hat{T}\hat{T})_0$ .

#### Analysis of the relaxation rates with the magnetic field and with the SF kinetics rates

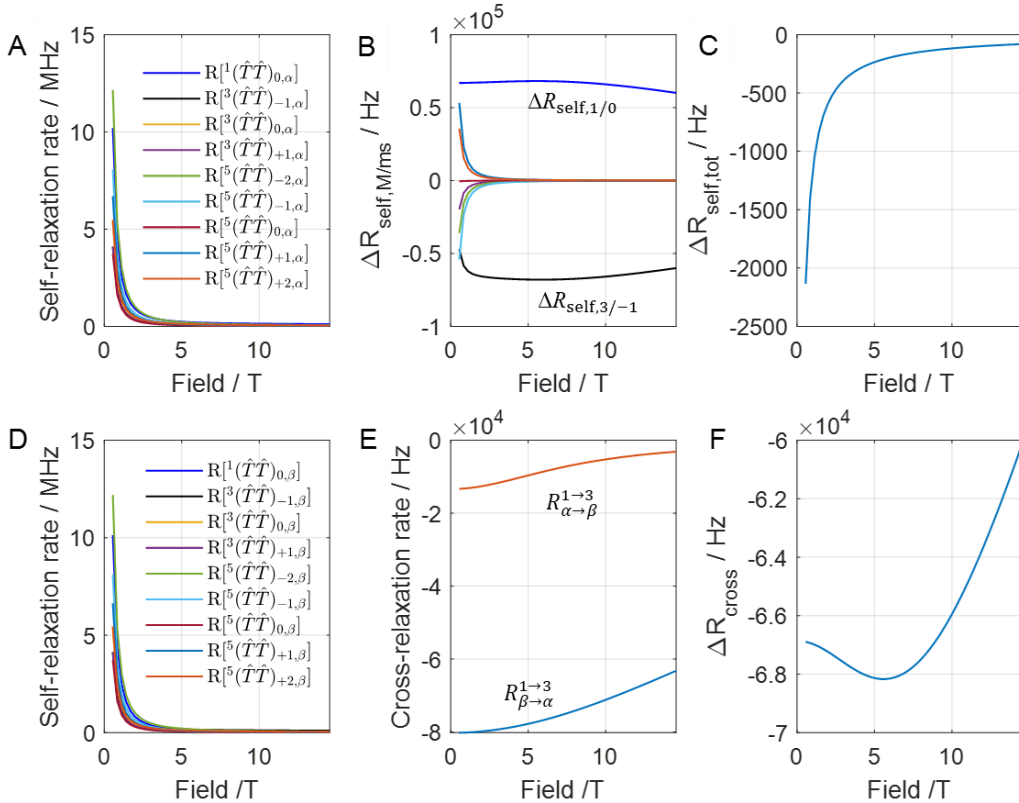


**Figure 4:** Self- and cross-relaxation rates as functions of the magnetic field. (A and D) Self-relaxation rates of the  $\alpha$  and  $\beta$  nuclear components of the triplet pair states. (B) The difference of self-relaxation rates ( $\Delta R_{\text{self,M/ms}}$ ) of the triplet pair states. The color code is the same used to indicate the triplet pair states in the figures (A) and (D). (C) The

difference between the sum of self-relaxation rates of all the triplet pair states, indicated with  $\Delta R_{\text{self,tot}}$ . (E) The cross-relaxation rates  $R_{\alpha \rightarrow \beta}^{1 \rightarrow 3}$  and  $R_{\beta \rightarrow \alpha}^{1 \rightarrow 3}$  and (F) the difference between the cross-relaxation rates  $\Delta R_{\text{cross}} = R_{\alpha \rightarrow \beta}^{1 \rightarrow 3} - R_{\beta \rightarrow \alpha}^{1 \rightarrow 3}$ .  $J_{\text{ex}}$  was set at the JDNP condition  $J_{\text{ex}} \approx \omega_E$ , and the other simulation parameters are given in Table 1.

We evaluated both the triplet-to-triplet cross- and self-relaxation rates as functions of the magnetic field (see Figure 4). Figures 4A and 4D show the decrease of the self-relaxation rates of the  $\alpha$  and  $\beta$  nuclear components of the triplet pair states with the magnetic field. The  $\Delta R_{\text{self,M/ms}}$  and  $\Delta R_{\text{self,tot}}$ , generally decay to zero with the magnetic field, except for  $\Delta R_{\text{self,1/0}}$  and  $\Delta R_{\text{self,3/-1}}$  associated with the states  $^1(\hat{T}\hat{T})_0$  and  $^3(\hat{T}\hat{T})_{-1}$  (see Figures 4B and 4C). Nevertheless, the self-relaxation processes contribute little to the nuclear polarization as the magnitude of total difference is two orders of magnitude smaller than that of the cross-relaxation. The  $R_{\alpha \rightarrow \beta}^{1 \rightarrow 3}$  and  $R_{\beta \rightarrow \alpha}^{1 \rightarrow 3}$  rates decrease slightly with the magnetic field (see Figures 4E and 4F) and the  $\Delta R_{\text{cross}}$  shows a small negative maximum at  $\sim 5$  T (for the parameter set used in the calculation).

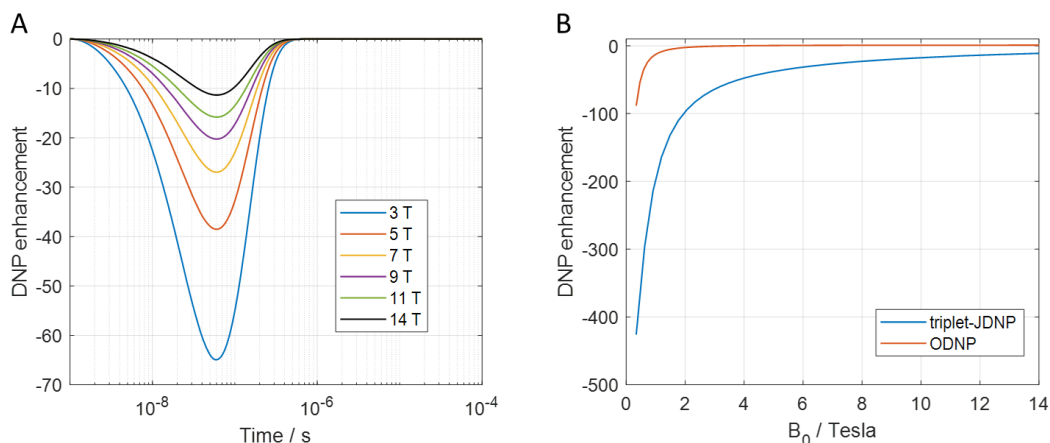


**Figure 5:** (A) Time-domain simulations showing the evolution of the  $^1\text{H}$  DNP enhancement in time as a function of the magnetic field. (B) Comparison between the maximum enhancement obtained in the triplet-JDNP time-domain simulations and that in steady-state  $^1\text{H}$  ODNP simulations (arising from dipolar interactions), as a function of the magnetic field.  $J_{\text{ex}}$  was set at the JDNP conditions  $J_{\text{ex}} \approx \omega_E$ , and the other simulation parameters are given in Table 1

With the set photo-kinetics of the pentacene dimer, the DNP enhancement reaches its maximum at  $\sim 50$  ns (considering the kinetics rates given in Table 1) and the DNP dynamics does not change with the magnetic field (Figure 5A). We observed a decrease of the DNP enhancement from 3 T to 14 T (see Figure 5B). Nevertheless, the enhancement factor of triplet-JDNP is much greater than ODNP (simulated considering one proton that is coupled to one electron with the dipolar hyperfine interaction) at the same magnetic field. Once the state  $^1(\hat{T}\hat{T})_0$  is created, the  $\hat{T}\hat{T}_{\alpha/\beta}$  states are populated due to self-relaxation  $R[\hat{M}\hat{T}\hat{T}_{m_s,\alpha/\beta}]$ . Subsequently, cross-relaxation rates  $R_{\alpha \rightarrow \beta}^{1 \rightarrow 3}$  and  $R_{\beta \rightarrow \alpha}^{1 \rightarrow 3}$  take place to create the population

imbalance of the nuclear spin. Although the cross-relaxation rates remain constant with the magnetic field, the self-relaxation rates decay with the magnetic field. Thereby, the  $\hat{T}\hat{T}_{\alpha/\beta}$  states will be less populated at the higher fields, and consequently the DNP enhancement is reduced.

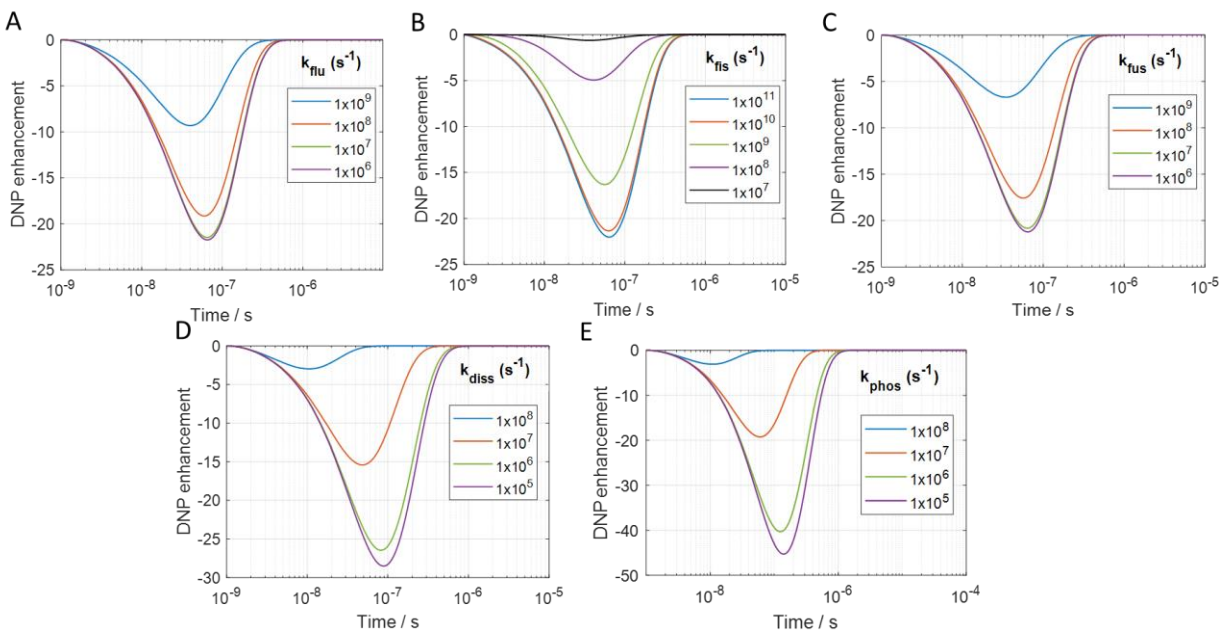


**Figure 6.** Effects of the kinetic rates on the DNP enhancement: (A)  $k_{\text{flu}}$ , (B)  $k_{\text{fis}}$ , (C)  $k_{\text{fus}}$ , (D)  $k_{\text{diss}}$  and (E)  $k_{\text{phos}}$ . Simulations were performed at 9.4 T. While one kinetics rate is changed, the other rates and parameters were kept the same as those shown in Table 1.

In order to provide insights for the design of an optimal polarizing agent for triplet-JDNP, we investigated the effects of the kinetics rates on the DNP enhancement. We analyzed the effect of the kinetics rates on a hypothetical pentacene dimer molecule that can fulfill the JDNP condition ( $J_{\text{ex}} \approx \omega_{\text{E}} = 263$  GHz) at a high magnet field (e.g. 9.4 T). We also showed the effect of the kinetics rates as a function of the  $J_{\text{ex}}$ , see the supporting material. In Figure 6, we observed an increase of the DNP enhancement with the decrease of  $k_{\text{flu}}$  that creates  $\hat{S}_1\hat{S}_0$  exciton and an increase of  $k_{\text{fis}}$  that generates the triplet pair state  $^1(\hat{T}\hat{T})_0$ . The DNP enhancement increases also with the decrease of  $k_{\text{diss}}$ ,  $k_{\text{fus}}$  and  $k_{\text{phos}}$  which subtracts population from the triplet pair states. The favorable conditions can be found for  $k_{\text{flu}} \leq 10^7$  s<sup>-1</sup>,  $k_{\text{fis}} \geq 10^9$  s<sup>-1</sup>,  $k_{\text{diss}} \leq 10^6$  s<sup>-1</sup>,  $k_{\text{fus}} \leq 10^7$  s<sup>-1</sup> and  $k_{\text{phos}} \leq 10^6$  s<sup>-1</sup>. In general,  $k_{\text{flu}}$  of the potential molecule has to be of the same magnitude or lower than  $k_{\text{fis}}$  to obtain a substantial population of  $\hat{S}_1\hat{S}_0$  and  $^1(\hat{T}\hat{T})_0$ . In turn,  $k_{\text{fis}}$ , and the self-relaxation rates  $\Delta R_{\text{self,M/ms}}$  have to be at least comparable to  $k_{\text{fus}}$ ,  $k_{\text{diss}}$  and  $k_{\text{phos}}$  to increase the population of the triplet pair states contributing to the DNP enhancement. Under the considered range of photo-kinetic rates, and if the JDNP condition can be fulfilled at a selected magnetic field, triplet-JDNP may achieve DNP enhancements between 20~50 at 9.4 T and between 10~30 at 14 T (Figure 7).

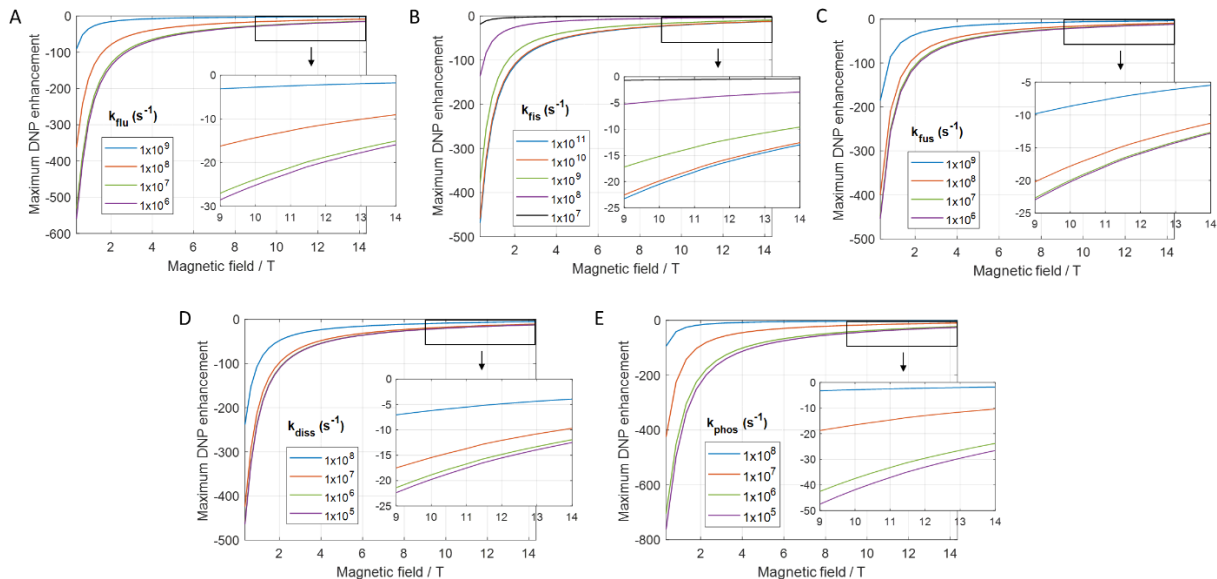


**Figure 7.** Maximum enhancement obtained in the triplet-JDNP simulations when  $J_{\text{ex}}$  is set to match the JDNP condition under variable kinetic rates: (A)  $k_{\text{flu}}$ , (B)  $k_{\text{fis}}$ , (C)  $k_{\text{fus}}$ , (D)  $k_{\text{diss}}$  and (E)  $k_{\text{phos}}$ . While one kinetics rate is changed, the other rates and parameters were kept the same as those shown in Table 1.

## Conclusion and outlooks:

We have explored the possibility of using non-conjugated pentacene dimers as polarizing agents for triplet-JDNP, which exploits the SF process to enhance the sensitivity of solution-state NMR's without microwaves. The simulated SF dynamics is consistent with that observed in transient absorption spectroscopy and TREPR experiments. At the JDNP condition ( $J_{\text{ex}} \approx \omega_{\text{E}}$ ), there is a level anti-crossing between the states  $^1(\hat{T}\hat{T})_0$  and  $^3(\hat{T}\hat{T})_{-1}$  and triplet-to-triplet cross-relaxation takes place. A difference between these rates leads to an imbalance between the  $\alpha$  and  $\beta$  nuclear components of the triplet pair states, and consequently to the creation of nuclear polarization. The DNP enhancement depends on the SF rates, and it can be enhanced with faster  $k_{\text{fis}}$  that creates triplet pair states and slower  $k_{\text{flu}}$ ,  $k_{\text{fus}}$ ,  $k_{\text{diss}}$ ,  $k_{\text{phos}}$  that depopulate the triplet pair states. The SF process, although happening on the ns timescale, is sufficiently long to polarize a single solvent molecule. In a real experiment, the bulk solvent can be polarized by photoexciting the sample continuously. Triplet-JDNP can be also performed at high magnetic fields ( $\geq 7$  T), if  $J_{\text{ex}}$  of the triplets can be increased. The requested  $J_{\text{ex}}$  values might be achieved by linking pentacene units with conjugated linkers containing para-phenylene / acetylene units, leading to  $J_{\text{ex}}$ (s) in the order of 100(s) GHz. The inter-electron exchange coupling can be measured from the magnetic field effects obtained in steady-state fluorescence measurements performed on frozen solutions at high magnetic fields up to 10 T. [51, 52] Like the JDNP, triplet-JDNP requires symmetric dimers with identical chromophore monomers. The  $g$ -tensor non-collinearity arising from vibrational modes and rotations does not suppress the DNP

enhancement (see the supporting material). The expected advantage of the triplet-JDNP over the other hyperpolarization methods, including ODNP, CIDNP and parahydrogen-induced polarization (PHIP), [53] is the broader applicability to  $^1\text{H}/^{13}\text{C}$  spectroscopy of a wider range of analytes, the possibility to use at higher magnetic fields, and the removal of microwave source. However, it still requires a JDNP condition to be fulfilled at a given field, and the optimal experimental conditions have to be determined. In the literature, there are many pentacene dimers that could suit for triplet-JDNP. [32, 42] The selection and optimization of various polarizing agents can be made trackable using transient optical absorption spectroscopy, photoluminescence experiments and TREPR.

The SF process was used previously to enhance solid-state NMR's sensitivity. [54] However, the polarization mechanism is different from the one proposed for triplet-JDNP. It exploited integrated solid effect (ISE) [26, 55] under microwave irradiation to transfer polarization from the electrons to the nuclei. A question arises about whether improvements can be obtained in solid-state DNP based on SF by employing triplet-pairs that fulfill the JDNP condition  $J_{\text{ex}} \approx \omega_{\text{E}}$ . Further theoretical work is ongoing to address this question.

#### **Acknowledgements:**

This project is supported by the National Natural Science Foundation of China (Nos. 22425402, 22275159 and 22273082), the Fundamental Research Funds for the Central Universities (YG2025ZD30) and the Open Project Fund of National Facility for Translational Medicine (Shanghai) (TMSK-2024-109). The authors acknowledge Prof. Zhitao Zhang and Prof. Lu Yu (High Magnetic Field Laboratory of Chinese Academy of Sciences); Miss Linlin Ma and Miss Ruibin Wang (Shanghai Jiao Tong University); Prof. Haiming Zhu, and Dr. Shuangshuang Li (Zhejiang University) for the preliminary experiments and discussions.

#### **Reference:**

1. Overhauser, A.W., *Polarization of nuclei in metals*. Physical Review, 1953. **92**(2): p. 411.
2. Carver, T.R. and C.P. Slichter, *Experimental verification of the Overhauser nuclear polarization effect*. Physical Review, 1956. **102**(4): p. 975.
3. Hausser, K.H. and D. Stehlik, *Dynamic nuclear polarization in liquids*, in *Advances in Magnetic and Optical Resonance*. Vol. 3. 1968: Elsevier.
4. Hausser, K.H. and D. Stehlik, *Dynamic nuclear polarization in liquids*, in *Advances in Magnetic and Optical Resonance*. 1968, Elsevier. p. 79-139.
5. Loening, N.M., et al., *Solution-state dynamic nuclear polarization at high magnetic field*. Journal of the American Chemical Society, 2002. **124**(30): p. 8808-8809.
6. Griesinger, C., et al., *Dynamic nuclear polarization at high magnetic fields in liquids*. Progress in Nuclear Magnetic Resonance Spectroscopy, 2012. **64**: p. 4-28.
7. Orlando, T., et al., *Dynamic Nuclear Polarization of  $^{13}\text{C}$  Nuclei in the Liquid State over a 10 Tesla Field Range*. Angewandte Chemie-International Edition, 2019. **58**(5): p. 1402-1406.
8. Höfer, P., et al., *Field dependent dynamic nuclear polarization with radicals in aqueous solution*. Journal of the American Chemical Society, 2008. **130**(11): p. 3254-+.

9. Liu, G.Q., et al., *One-thousand-fold enhancement of high field liquid nuclear magnetic resonance signals at room temperature*. *Nature Chemistry*, 2017. **9**(7): p. 676-680.
10. Parigi, G., et al., *Unveiling protein dynamics in solution with field-cycling NMR relaxometry*. *Progress in Nuclear Magnetic Resonance Spectroscopy*, 2021. **124**: p. 85-98.
11. Dai, D.H., et al., *Room-temperature dynamic nuclear polarization enhanced NMR spectroscopy of small biological molecules in water*. *Nature Communications*, 2021. **12**(1).
12. Levien, M., et al., *Nitroxide Derivatives for Dynamic Nuclear Polarization in Liquids: The Role of Rotational Diffusion*. *Journal of Physical Chemistry Letters*, 2020. **11**(5): p. 1629-1635.
13. Yoon, D., et al., *High-Field Liquid-State Dynamic Nuclear Polarization in Microliter Samples*. *Analytical Chemistry*, 2018. **90**(9): p. 5620-5626.
14. Dubroca, T., et al., *A quasi-optical and corrugated waveguide microwave transmission system for simultaneous dynamic nuclear polarization NMR on two separate 14.1 T spectrometers*. *Journal of Magnetic Resonance*, 2018. **289**: p. 35-44.
15. Mullerwarmuth, W. and K. Meisegresch, *Molecular Motions and Interactions as Studied by Dynamic Nuclear-Polarization (Dnp) in Free-Radical Solutions*. *Advances in Magnetic Resonance*, 1983. **11**: p. 1-45.
16. Orlando, T., I. Kuprov, and M. Hiller, *Theoretical analysis of scalar relaxation in <sup>13</sup>C-DNP in liquids*. *Journal of Magnetic Resonance Open*, 2022. **10-11**.
17. Ardenkjær-Larsen, J.H., et al., *EPR and DNP properties of certain novel single electron contrast agents intended for oximetric imaging*. *Journal of Magnetic Resonance*, 1998. **133**(1): p. 1-12.
18. Wind, R.A. and J.H. Ardenkjær-Larsen, *H DNP at 1.4 T of water doped with a triarylmethyl-based radical*. *Journal of Magnetic Resonance*, 1999. **141**(2): p. 347-354.
19. Levien, M., et al., *Spin density localization and accessibility of organic radicals affect liquid-state DNP efficiency*. *Physical Chemistry Chemical Physics*, 2021. **23**(8): p. 4480-4485.
20. Concilio, M.G., I. Kuprov, and L. Frydman, *-Driven dynamic nuclear polarization for sensitizing high field solution state NMR*. *Physical Chemistry Chemical Physics*, 2022. **24**(4): p. 2118-2125.
21. Concilio, M.G. and L. Frydman, *Steady state effects introduced by local relaxation modes on J-driven DNP-enhanced NMR*. *Journal of Magnetic Resonance*, 2023. **355**.
22. J. Bargon, H.F.a.U.J., *Kernresonanz-Emissionslinien während rascher Radikalreaktionen*. *Zeitschrift für Naturforschung A*, 1967(22): p. 1551.
23. Kaptein, R. and J.L. Oosterhoff, *Chemically induced dynamic nuclear polarization II - (Relation with anomalous ESR spectra)*. *Chemical Physics Letters*, 1969. **4**(4): p. 195-197.
24. Closs, G.L., *A Mechanism Explaining Nuclear Spin Polarizations in Radical Combination Reactions*. *Journal of the American Chemical Society*, 1969. **91**(16): p. 4552-&.
25. Santabarbara, S., et al., *Bidirectional Electron Transfer in Photosystem I: Determination of Two Distances between P700+ and A1- in Spin-Correlated Radical Pairs*. *Biochemistry*, 2005. **44**(6): p. 2119-2128.
26. Nishimura, K., et al., *Materials chemistry of triplet dynamic nuclear polarization*. *Chemical Communications*, 2020. **56**(53): p. 7217-7232.
27. Yabuki, R., et al., *Dynamic electron and nuclear spin polarization in solution using porphyrin and tris(2,4,6-trichlorophenyl)-methyl (TTM) radical derivatives*. *Journal of Magnetic Resonance Open*, 2025. **22**.
28. Smith, M.B. and J. Michl, *Singlet Fission*. *Chemical Reviews*, 2010. **110**(11): p. 6891-6936.
29. Smith, M.B. and J. Michl, *Recent Advances in Singlet Fission*. *Annual Review of Physical Chemistry*, Vol 64, 2013. **64**: p. 361-386.
30. Wang, L.J., et al., *Maximizing Singlet Fission by Intermolecular Packing*. *Journal of Physical Chemistry Letters*, 2014. **5**(19): p. 3345-3353.
31. Basel, B.S., et al., *Unified model for singlet fission within a non-conjugated covalent pentacene dimer*. *Nature Communications*, 2017. **8**.
32. Basel, B.S., et al., *Evidence for Charge-Transfer Mediation in the Primary Events of Singlet Fission in a Weakly Coupled Pentacene Dimer*. *Chem*, 2018. **4**(5): p. 1092-1111.

33. Redfield, A., *The theory of relaxation processes*, in *Advances in Magnetic and Optical Resonance*. 1965, Elsevier. p. 1-32.
34. Breuer, H. and F. Petruccione, *The Theory of Open Quantum Systems* (Oxford University Press, Oxford).
35. Wangsness, R.K. and F. Bloch, *The dynamical theory of nuclear induction*. *Physical Review*, 1953. **89**(4): p. 728.
36. Kuprov, I., N. Wagner-Rundell, and P. Hore, *Bloch-Redfield-Wangsness theory engine implementation using symbolic processing software*. *Journal of Magnetic Resonance*, 2007. **184**(2): p. 196-206.
37. Ito, F., et al., *Carrier generation process on photoconductive polymer films as studied by magnetic field effects on the charge-transfer fluorescence and photocurrent*. *Journal of Physical Chemistry B*, 2005. **109**(18): p. 8707-8717.
38. Yago, T., et al., *Magnetic Field Effects on Triplet Pair Generated by Singlet Fission in an Organic Crystal: Application of Radical Pair Model to Triplet Pair*. *Journal of Physical Chemistry C*, 2016. **120**(49): p. 27858-27870.
39. Vanstrien, A.J. and J. Schmidt, *An Electron-Paramagnetic-Res Study of the Triplet-State of Pentacene by Electron Spin-Echo Techniques and Laser Flash Excitation*. *Chemical Physics Letters*, 1980. **70**(3): p. 513-517.
40. Avalos, C.E., et al., *Enhanced Intersystem Crossing and Transient Electron Spin Polarization in a Photoexcited Pentacene-Triptyl Radical*. *Journal of Physical Chemistry A*, 2020. **124**(29): p. 6068-6075.
41. Tayebjee, M.J.Y., et al., *Quintet multiexciton dynamics in singlet fission*. *Nature Physics*, 2017. **13**(2): p. 182-188.
42. Majumder, K., et al., *Controlling Intramolecular Singlet Fission Dynamics via Torsional Modulation of Through-Bond versus Through-Space Couplings*. *Journal of the American Chemical Society*, 2023. **145**(38): p. 20883-20896.
43. Schott, S., et al., *Tuning the effective spin-orbit coupling in molecular semiconductors*. *Nature Communications*, 2017. **8**.
44. Hogben, H., et al., *Spinach - a software library for simulation of spin dynamics in large spin systems*. *Journal of Magnetic Resonance*, 2011. **208**(2): p. 179-194.
45. Sanders, S.N., et al., *Understanding the Bound Triplet-Pair State in Singlet Fission*. *Chem*, 2019. **5**(8): p. 1988-2005.
46. Piland, G.B., et al., *Singlet Fission: From Coherences to Kinetics*. *Journal of Physical Chemistry Letters*, 2014. **5**(13): p. 2312-2319.
47. Basel, B.S., et al., *Influence of the heavy-atom effect on singlet fission: a study of platinum-bridged pentacene dimers*. *Chemical Science*, 2019. **10**(48): p. 11130-11140.
48. Merrifield, R.E., *Theory of Magnetic Field Effects on the Mutual Annihilation of Triplet Excitons*. *J. Chem. Phys.*, 1968(48): p. 4318– 431921.
49. Wang, Z.W., et al., *Free-triplet generation with improved efficiency in tetracene oligomers through spatially separated triplet pair states*. *Nature Chemistry*, 2021. **13**(6): p. 559-+.
50. Blicharski, J., *Nuclear magnetic relaxation by anisotropy of the chemical shift*. *Z Naturforsch Pt A*, 1972. **27**: p. 1456-1458.
51. Xu, R., C.F. Zhang, and M. Xiao, *Review Magnetic field effects on singlet fission dynamics*. *Trends in Chemistry*, 2022. **4**(6): p. 528-539.
52. Bayliss, S.L., et al., *Spin signatures of exchange-coupled triplet pairs formed by singlet fission*. *Physical Review B*, 2016. **94**(4).
53. Hövener, J.B., et al., *Parahydrogen-Based Hyperpolarization for Biomedicine*. *Angewandte Chemie-International Edition*, 2018. **57**(35): p. 11140-11162.
54. Kawashima, Y., et al., *Singlet fission as a polarized spin generator for dynamic nuclear polarization*. *Nature Communications*, 2023. **14**(1).

55. Henstra, A., et al., *High Dynamic Nuclear-Polarization at Room-Temperature*. Chemical Physics Letters, 1990. **165**(1): p. 6-10.

## Supplementary material for

### Triplet J-driven DNP – a proposal to increase the sensitivity of solution state NMR without microwave

Maria Grazia Concilio<sup>1\*</sup>, Yiwen Wang<sup>1</sup>, and Linjun Wang<sup>2,3</sup>, Xueqian Kong<sup>1,2\*</sup>

<sup>1</sup>*Institute of Translational Medicine, Shanghai Jiao Tong University, 200240 Shanghai, China*

<sup>2</sup>*Department of Chemistry, Zhejiang University, 310058 Hangzhou, Zhejiang, China*

<sup>3</sup>*Zhejiang Key Laboratory of Excited-State Energy Conversion and Energy Storage, Department of Chemistry, Zhejiang University, 310058 Hangzhou, Zhejiang, China*

#### Contents

- A. Magnetic field effect on the SF kinetics
- B. Effect of the self-relaxation rates on the DNP enhancement
- C. Spectral density functions representing the self-relaxation rates
- D. Effects of the kinetic rates and of the  $J_{\text{ex}}$  on the DNP enhancement
- E. Effect of anisotropic  $g$ -tensors on the self-relaxation rates and on the DNP enhancement

### A. Magnetic field effect on the SF kinetics:

To determine the magnitude of the kinetics constants  $k_{\text{fis}} = k_{\text{fis}} |C_{\text{singlet}}^l|^2$  and  $k_{\text{fus}} = k_{\text{fus}} |C_{\text{singlet}}^l|^2$ , and of the singlet character  $C_{\text{singlet}}^l = \langle {}^1(\hat{T}\hat{T})_0 | \varphi_l \rangle$  ( $l = 1-9$ ), we computed the eigenstates  $\varphi_l$  of the Hamiltonian in Eq. 6 in the main text, and calculated the projections of the nine sublevels on the singlet state  ${}^1(\hat{T}\hat{T})_0$  in according to  $|C_{\text{singlet}}^l|^2$  at different magnetic fields (Figure S1):

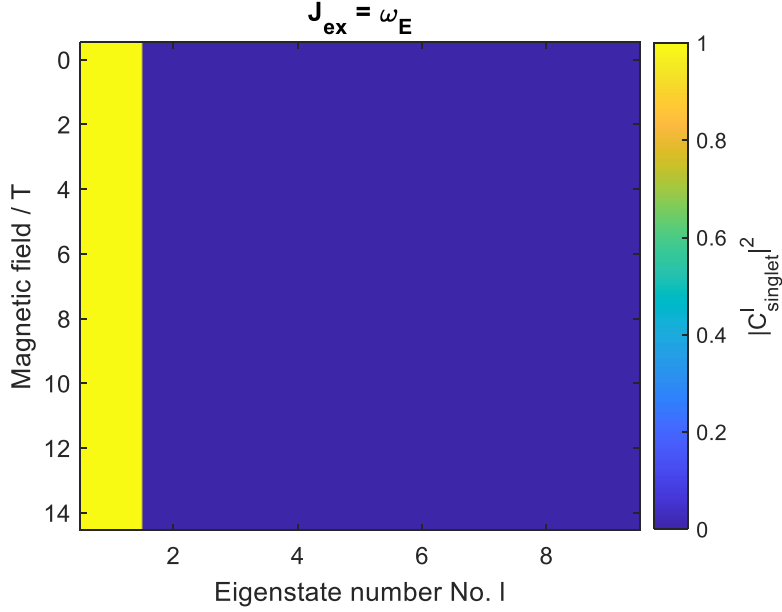


**Figure S1.** Spin projections of the nine triplet pair eigenstates on the singlet state, as a function of the magnetic field.

In the case of strongly coupled triplet pairs ( $J_{\text{ex}} \approx \text{GHz}$ ) and in the absence of the anisotropic part of the spin interactions, the  $C_{\text{singlet}}^l$  is equal to 1 and the SF kinetics rates are not expected to change with the magnetic field.

## B. Effect of the self-relaxation rates on the DNP enhancement

A difference between the self-relaxation rates of the  $\alpha$  and  $\beta$  nuclear components of the triplet pair states,  $\Delta R_{\text{self,M/ms}}$  is not expected to contribute to the DNP enhancement. The self-relaxation rates of individual triplet pairs have positive and negative magnitude (Figure S2A and S2B), resulting in a difference between the sum of the  $\alpha$  and  $\beta$  self-relaxation rates, indicated as  $\Delta R_{\text{self,tot}}$ , with negative magnitude longer than the timescale of the SF process see Figure S2C:

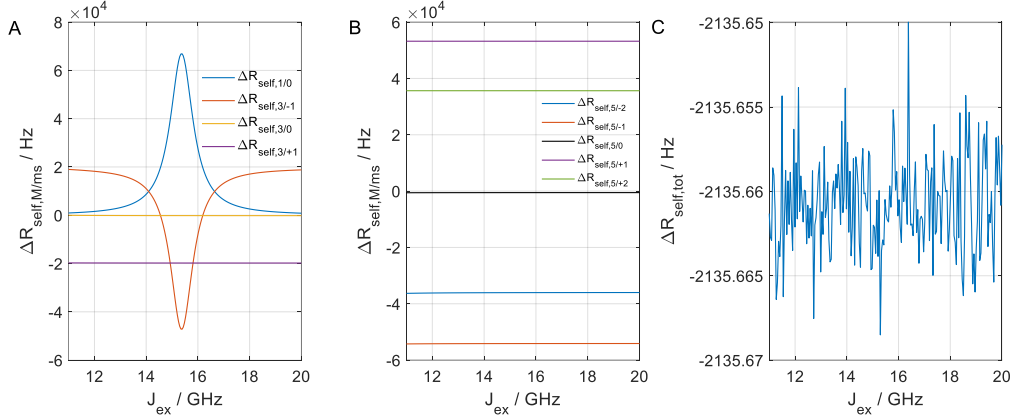


**Figure S2:** (A and B) The difference between the self-relaxation rates of the triplet pair state. (C) The difference between the sum of the self-relaxation rates of the triplet pair states, as a function of the  $J_{\text{ex}}$ . Simulations were performed at 0.55 T. The other simulation parameters are given in the Table 1.

When JDNP condition is fulfilled (at about 15 GHz, see Figure S2), the self-relaxation rates remain constant with the  $J_{\text{ex}}$  except the states  $^1(\hat{T}\hat{T})_0$  and  $^3(\hat{T}\hat{T})_{-1}$ . The modulations in the self-relaxation rates of  $^1(\hat{T}\hat{T})_0$  and  $^3(\hat{T}\hat{T})_{-1}$  states are due to the presence of the terms  $J(J_{\text{ex}} \mp \omega_E \mp \omega_N)$  and  $J(J_{\text{ex}} \pm \omega_E \mp \omega_N)$  in the spectral density functions, given in Eq. S2 – S10 in the supporting material.  $\Delta R_{\text{self,tot}}$  arises mostly from the states  $^1(\hat{T}\hat{T})_0$  and  $^3(\hat{T}\hat{T})_{-1}$ . Eq. S1 shows the spectral density function of  $\Delta R_{\text{self,tot}}$  of the triplet pair states:

$$\Delta R_{\text{self,tot}} = \left[ \begin{aligned} & \frac{4}{405}J(J_{\text{ex}} - \omega_N) + \frac{4}{405}J(J_{\text{ex}} + \omega_N) + \frac{1}{81}J(2J_{\text{ex}} - \omega_N) + \frac{1}{81}J(2J_{\text{ex}} + \omega_N) + \\ & \frac{8}{405}J(J_{\text{ex}} - \omega_E - \omega_N) + \frac{8}{405}J(J_{\text{ex}} + \omega_E + \omega_N) + \frac{2}{81}J(2J_{\text{ex}} - \omega_E - \omega_N) + \\ & \frac{2}{81}J(2J_{\text{ex}} + \omega_E + \omega_N) + \frac{4}{1215}J(J_{\text{ex}} + \omega_E - \omega_N) + \frac{4}{1215}J(J_{\text{ex}} - \omega_E + \omega_N) + \\ & \quad + \frac{1}{243}J(2J_{\text{ex}} - \omega_E + \omega_N) + \frac{1}{243}J(2J_{\text{ex}} + \omega_E - \omega_N) \end{aligned} \right] \Delta_{\text{HFC}_1 - \text{HFC}_2}^2 + \left[ \frac{14}{135}J(\omega_E) + \frac{2}{45}J(\omega_N) \right] \Delta_{\text{HFC}_1 + \text{HFC}_2}^2 \quad (\text{S1})$$

where the terms  $\Delta_{\text{HFC}_1 + \text{HFC}_2}^2$  is a matrix corresponding to the second rank norm squared arising from the sum of the anisotropy of the two dipolar hyperfine tensors [50].  $\Delta R_{\text{self,tot}}$  is dominated by the term containing  $\Delta_{\text{HFC}_1 + \text{HFC}_2}^2 J(\omega_N)$  that does not depend on the  $J_{\text{ex}}$ , this explains the stability of  $\Delta R_{\text{self,tot}}$  with the  $J_{\text{ex}}$  in the Figure S2.

### C. Spectral density functions representing the self-relaxation rates:

In the case of  ${}^1(\hat{T}\hat{T})_0$ , the rate corresponds to:

$$\begin{aligned}
\Delta R_{self,1/0} &= R \left[ {}^1(\hat{T}\hat{T})_{0,\alpha} \right] - R \left[ {}^1(\hat{T}\hat{T})_{0,\beta} \right] \\
&\approx \frac{32}{135} (\aleph_{G1,HFC1} - \aleph_{G1,HFC2} - \aleph_{G2,HFC1} + \aleph_{G2,HFC2}) [J(J_{ex})] + \\
&\quad \frac{8}{45} (\aleph_{G1,HFC1} - \aleph_{G1,HFC2} - \aleph_{G2,HFC1} + \aleph_{G2,HFC2}) [J(J_{ex} - \omega_E) + J(J_{ex} + \omega_E)] + \\
&\quad \frac{4}{45} \Delta_{HFC1-HFC2}^2 [J(J_{ex} - \omega_E - \omega_N) - J(J_{ex} + \omega_E + \omega_N)] + \\
&\quad \frac{2}{135} \Delta_{HFC1-HFC2}^2 [J(J_{ex} + \omega_E - \omega_N) - J(J_{ex} - \omega_E + \omega_N)] + \\
&\quad \frac{2}{45} \Delta_{HFC1-HFC2}^2 [J(J_{ex} - \omega_N) - J(J_{ex} + \omega_N)]
\end{aligned} \tag{S2}$$

In the case of  ${}^3(\hat{T}\hat{T})_0$ , the rate corresponds to:

$$\begin{aligned}
\Delta R_{self,3/0} &= R \left[ {}^3(\hat{T}\hat{T})_{0,\alpha} \right] - R \left[ {}^3(\hat{T}\hat{T})_{0,\beta} \right] \\
&\approx \frac{32}{135} (\aleph_{G1,HFC1} - \aleph_{G1,HFC2} - \aleph_{G2,HFC1} + \aleph_{G2,HFC2}) [J(J_{ex})] + \\
&\quad \frac{16}{135} (\aleph_{G1,HFC1} - \aleph_{G1,HFC2} - \aleph_{G2,HFC1} + \aleph_{G2,HFC2}) [J(2J_{ex})] + \\
&\quad \frac{1}{45} \Delta_{HFC1-HFC2}^2 [J(2J_{ex} - \omega_N) - J(2J_{ex} + \omega_N)] + \\
&\quad \frac{2}{45} \Delta_{HFC1-HFC2}^2 [J(J_{ex} + \omega_N) - J(J_{ex} - \omega_N)] + \\
&\quad \frac{1}{15} \left( \aleph_{G1,HFC1} - \aleph_{G1,HFC2} - \aleph_{G2,HFC1} + \aleph_{G2,HFC2} + \right. \\
&\quad \left. \aleph_{ZFS1,HFC1} - \aleph_{ZFS2,HFC1} - \aleph_{ZFS1,HFC2} + \aleph_{ZFS2,HFC2} \right) [J(2J_{ex} - \omega_E)] + \\
&\quad \frac{1}{15} \left( \aleph_{G1,HFC1} - \aleph_{G1,HFC2} - \aleph_{G2,HFC1} + \aleph_{G2,HFC2} - \right. \\
&\quad \left. \aleph_{ZFS1,HFC1} + \aleph_{ZFS2,HFC1} + \aleph_{ZFS1,HFC2} - \aleph_{ZFS2,HFC2} \right) [J(2J_{ex} + \omega_E)] + \\
&\quad \frac{1}{30} \Delta_{HFC1-HFC2}^2 [J(2J_{ex} - \omega_E - \omega_N) - J(2J_{ex} + \omega_E + \omega_N)] + \\
&\quad \frac{1}{180} \Delta_{HFC1-HFC2}^2 [J(2J_{ex} + \omega_E - \omega_N) - J(2J_{ex} - \omega_E + \omega_N)] + \dots
\end{aligned} \tag{S3}$$

In the case of  ${}^3(\hat{T}\hat{T})_{\pm 1}$ , the rate corresponds to:

$$\begin{aligned}
\Delta R_{self,3/+1} &= R \left[ {}^3(\hat{T}\hat{T})_{+1,\alpha} \right] - R \left[ {}^3(\hat{T}\hat{T})_{+1,\beta} \right] \\
&\approx \frac{4}{45} (\aleph_{G1,HFC1} - \aleph_{G1,HFC2} - \aleph_{G2,HFC1} + \aleph_{G2,HFC2}) [J(2J_{ex})] + \\
&\quad \frac{2}{15} (\aleph_{ZFS1,HFC1} - \aleph_{ZFS1,HFC2} - \aleph_{ZFS2,HFC1} + \aleph_{ZFS2,HFC2}) [J(2J_{ex})] + \\
&\quad \frac{1}{45} \left( \aleph_{G1,HFC1} - \aleph_{G1,HFC2} - \aleph_{G2,HFC1} + \aleph_{G2,HFC2} + \right. \\
&\quad \left. 3\aleph_{ZFS1,HFC1} - 3\aleph_{ZFS1,HFC2} - 3\aleph_{ZFS2,HFC1} + 3\aleph_{ZFS2,HFC2} \right) [J(2J_{ex} - \omega_E)] + \\
&\quad \frac{2}{15} \left( \aleph_{G1,HFC1} - \aleph_{G1,HFC2} - \aleph_{G2,HFC1} + \aleph_{G2,HFC2} + \right. \\
&\quad \left. \aleph_{ZFS1,HFC1} - \aleph_{ZFS1,HFC2} - \aleph_{ZFS2,HFC1} + \aleph_{ZFS2,HFC2} \right) [J(2J_{ex} + \omega_E)] +
\end{aligned}$$

$$\begin{aligned}
& \frac{8}{45} (\aleph_{G1,HFC1} - \aleph_{G1,HFC2} - \aleph_{G2,HFC1} + \aleph_{G2,HFC2}) [J(J_{ex} + \omega_E)] + \\
& \frac{1}{90} \Delta_{HFC1-HFC2}^2 [J(2J_{ex} - \omega_E - \omega_N)] - \frac{1}{15} \Delta_{HFC1-HFC2}^2 [J(2J_{ex} + \omega_E + \omega_N)] + \\
& \frac{1}{90} \Delta_{HFC1-HFC2}^2 [J(2J_{ex} + \omega_E - \omega_N)] - \frac{1}{540} \Delta_{HFC1-HFC2}^2 [J(2J_{ex} - \omega_E + \omega_N)] + \\
& \frac{4}{45} \Delta_{HFC1-HFC2}^2 [J(J_{ex} + \omega_E + \omega_N)] - \frac{2}{135} \Delta_{HFC1-HFC2}^2 [J(J_{ex} + \omega_E - \omega_N)] + \\
& \frac{1}{60} \Delta_{HFC1-HFC2}^2 [J(2J_{ex} - \omega_N) - J(2J_{ex} + \omega_N)] + \dots
\end{aligned} \tag{S4}$$

and:

$$\begin{aligned}
\Delta R_{\text{self},3/-1} &= R \left[ {}^3(\widehat{\text{T}\widehat{\text{T}}})_{-1,\alpha} \right] - R \left[ {}^3(\widehat{\text{T}\widehat{\text{T}}})_{-1,\beta} \right] \\
&\approx \frac{4}{45} (\aleph_{G1,HFC1} - \aleph_{G1,HFC2} - \aleph_{G2,HFC1} + \aleph_{G2,HFC2}) [J(2J_{ex})] + \\
& \frac{2}{15} (-\aleph_{ZFS1,HFC1} + \aleph_{ZFS1,HFC2} + \aleph_{ZFS2,HFC1} - \aleph_{ZFS2,HFC2}) [J(2J_{ex})] + \\
& \frac{1}{45} \left( \aleph_{G1,HFC1} - \aleph_{G1,HFC2} - \aleph_{G2,HFC1} + \aleph_{G2,HFC2} - \right. \\
& \left. 3\aleph_{ZFS1,HFC1} + 3\aleph_{ZFS1,HFC2} + 3\aleph_{ZFS2,HFC1} - 3\aleph_{ZFS2,HFC2} \right) [J(2J_{ex} + \omega_E)] + \\
& \frac{2}{15} \left( \aleph_{G1,HFC1} - \aleph_{G1,HFC2} - \aleph_{G2,HFC1} + \aleph_{G2,HFC2} - \right. \\
& \left. \aleph_{ZFS1,HFC1} + \aleph_{ZFS1,HFC2} + \aleph_{ZFS2,HFC1} - \aleph_{ZFS2,HFC2} \right) [J(2J_{ex} - \omega_E)] + \\
& \frac{8}{45} (\aleph_{G1,HFC1} - \aleph_{G1,HFC2} - \aleph_{G2,HFC1} + \aleph_{G2,HFC2}) [J(J_{ex} - \omega_E)] - \\
& \frac{1}{90} \Delta_{HFC1-HFC2}^2 [J(2J_{ex} - \omega_E + \omega_N)] + \frac{1}{15} \Delta_{HFC1-HFC2}^2 [J(2J_{ex} - \omega_E - \omega_N)] - \\
& \frac{1}{90} \Delta_{HFC1-HFC2}^2 [J(2J_{ex} + \omega_E + \omega_N)] - \frac{1}{540} \Delta_{HFC1-HFC2}^2 [J(2J_{ex} + \omega_E - \omega_N)] - \\
& \frac{4}{45} \Delta_{HFC1-HFC2}^2 [J(J_{ex} - \omega_E - \omega_N)] + \frac{2}{135} \Delta_{HFC1-HFC2}^2 [J(J_{ex} - \omega_E + \omega_N)] + \\
& \frac{1}{60} \Delta_{HFC1-HFC2}^2 [J(2J_{ex} - \omega_N) - J(2J_{ex} + \omega_N)] + \dots
\end{aligned} \tag{S5}$$

In the case of  ${}^5(\widehat{\text{T}\widehat{\text{T}}})_{\pm 1}$ , the rate corresponds to:

$$\begin{aligned}
\Delta R_{\text{self},5/+1} &= R \left[ {}^5(\widehat{\text{T}\widehat{\text{T}}})_{+1,\alpha} \right] - R \left[ {}^5(\widehat{\text{T}\widehat{\text{T}}})_{+1,\beta} \right] \\
&\approx \frac{4}{45} (\aleph_{G1,HFC1} - \aleph_{G1,HFC2} - \aleph_{G2,HFC1} + \aleph_{G2,HFC2}) [J(2J_{ex})] + \\
& \frac{2}{15} (\aleph_{ZFS1,HFC1} - \aleph_{ZFS1,HFC2} - \aleph_{ZFS2,HFC1} + \aleph_{ZFS2,HFC2}) [J(2J_{ex})] + \\
& \frac{1}{60} \Delta_{HFC1-HFC2}^2 [J(2J_{ex} + \omega_N) - J(2J_{ex} - \omega_N)] + \\
& \frac{1}{30} \Delta_{HFC1-HFC2}^2 [J(2J_{ex} + \omega_E + \omega_N)] - \frac{1}{180} \Delta_{HFC1-HFC2}^2 [J(2J_{ex} + \omega_E - \omega_N)] + \\
& \frac{1}{15} \left( \aleph_{G1,HFC1} - \aleph_{G1,HFC2} - \aleph_{G2,HFC1} + \aleph_{G2,HFC2} - \right. \\
& \left. \aleph_{ZFS1,HFC1} + \aleph_{ZFS1,HFC2} + \aleph_{ZFS2,HFC1} - \aleph_{ZFS2,HFC2} \right) [J(2J_{ex} + \omega_E)] + \dots
\end{aligned} \tag{S6}$$

and:

$$\begin{aligned}
\Delta R_{\text{self},5/-1} &= R \left[ {}^5(\widehat{\text{T}\widehat{\text{T}}})_{-1,\alpha} \right] - R \left[ {}^5(\widehat{\text{T}\widehat{\text{T}}})_{-1,\beta} \right] \\
&\approx \frac{4}{45} (\aleph_{G1,HFC1} - \aleph_{G1,HFC2} - \aleph_{G2,HFC1} + \aleph_{G2,HFC2}) [J(2J_{ex})] +
\end{aligned}$$

$$\begin{aligned}
& \frac{2}{15} (-\aleph_{\text{ZFS1,HFC1}} + \aleph_{\text{ZFS1,HFC2}} + \aleph_{\text{ZFS2,HFC1}} - \aleph_{\text{ZFS2,HFC2}}) [J(2J_{ex})] + \\
& \frac{1}{60} \Delta_{\text{HFC1-HFC2}}^2 [J(2J_{ex} + \omega_N) - J(2J_{ex} - \omega_N)] - \\
& \frac{1}{30} \Delta_{\text{HFC1-HFC2}}^2 [J(2J_{ex} - \omega_E - \omega_N)] + \frac{1}{180} \Delta_{\text{HFC1-HFC2}}^2 [J(2J_{ex} - \omega_E + \omega_N)] + \\
& \frac{1}{15} \left( \aleph_{\text{G1,HFC1}} - \aleph_{\text{G1,HFC2}} - \aleph_{\text{G2,HFC1}} + \aleph_{\text{G2,HFC2}} + \right. \\
& \left. \aleph_{\text{ZFS1,HFC1}} - \aleph_{\text{ZFS1,HFC2}} - \aleph_{\text{ZFS2,HFC1}} + \aleph_{\text{ZFS2,HFC2}} \right) [J(2J_{ex} - \omega_E)] + \dots
\end{aligned} \tag{S7}$$

In the case of  ${}^5(\hat{\text{T}}\hat{\text{T}})_0$ , the rate corresponds to:

$$\begin{aligned}
\Delta R_{\text{self},5/0} &= R \left[ {}^5(\hat{\text{T}}\hat{\text{T}})_{0,\alpha} \right] - R \left[ {}^5(\hat{\text{T}}\hat{\text{T}})_{0,\beta} \right] \\
&\approx \frac{16}{135} (\aleph_{\text{G1,HFC1}} - \aleph_{\text{G1,HFC2}} - \aleph_{\text{G2,HFC1}} + \aleph_{\text{G2,HFC2}}) [J(2J_{ex})] + \\
& \frac{1}{45} \Delta_{\text{HFC1-HFC2}}^2 [J(2J_{ex} + \omega_N) - J(2J_{ex} - \omega_N)] + \\
& \frac{1}{540} \Delta_{\text{HFC1-HFC2}}^2 [J(2J_{ex} - \omega_E + \omega_N) - J(2J_{ex} + \omega_E - \omega_N)] + \\
& \frac{1}{90} \Delta_{\text{HFC1-HFC2}}^2 [J(2J_{ex} + \omega_E + \omega_N) - J(2J_{ex} - \omega_E - \omega_N)] + \\
& \frac{1}{45} \left( \aleph_{\text{G1,HFC1}} - \aleph_{\text{G1,HFC2}} - \aleph_{\text{G2,HFC1}} + \aleph_{\text{G2,HFC2}} - \right. \\
& \left. 3\aleph_{\text{ZFS1,HFC1}} + 3\aleph_{\text{ZFS1,HFC2}} + 3\aleph_{\text{ZFS2,HFC1}} - 3\aleph_{\text{ZFS2,HFC2}} \right) [J(2J_{ex} + \omega_E)] + \\
& \frac{1}{45} \left( \aleph_{\text{G1,HFC1}} - \aleph_{\text{G1,HFC2}} - \aleph_{\text{G2,HFC1}} + \aleph_{\text{G2,HFC2}} + \right. \\
& \left. 3\aleph_{\text{ZFS1,HFC1}} - 3\aleph_{\text{ZFS1,HFC2}} - 3\aleph_{\text{ZFS2,HFC1}} + 3\aleph_{\text{ZFS2,HFC2}} \right) [J(2J_{ex} - \omega_E)] + \dots
\end{aligned} \tag{S8}$$

In the case of  ${}^5(\hat{\text{T}}\hat{\text{T}})_{\pm 2}$ , the rate corresponds to:

$$\begin{aligned}
\Delta R_{\text{self},5/+2} &= R \left[ {}^5(\hat{\text{T}}\hat{\text{T}})_{+2,\alpha} \right] - R \left[ {}^5(\hat{\text{T}}\hat{\text{T}})_{+2,\beta} \right] \\
&\approx \frac{1}{15} \Delta_{\text{HFC1-HFC2}}^2 [J(2J_{ex} + \omega_E + \omega_N)] - \frac{1}{90} \Delta_{\text{HFC1-HFC2}}^2 [J(2J_{ex} + \omega_E - \omega_N)] + \\
& \frac{2}{15} \left( \aleph_{\text{G1,HFC1}} - \aleph_{\text{G1,HFC2}} - \aleph_{\text{G2,HFC1}} + \aleph_{\text{G2,HFC2}} + \right. \\
& \left. \aleph_{\text{ZFS1,HFC1}} - \aleph_{\text{ZFS1,HFC2}} - \aleph_{\text{ZFS2,HFC1}} + \aleph_{\text{ZFS2,HFC2}} \right) [J(2J_{ex} + \omega_E)] + \dots
\end{aligned} \tag{S9}$$

and:

$$\begin{aligned}
\Delta R_{\text{self},5/-2} &= R \left[ {}^5(\hat{\text{T}}\hat{\text{T}})_{-2,\alpha} \right] - R \left[ {}^5(\hat{\text{T}}\hat{\text{T}})_{-2,\beta} \right] \\
&\approx -\frac{1}{15} \Delta_{\text{HFC1-HFC2}}^2 [J(2J_{ex} - \omega_E - \omega_N)] + \frac{1}{90} \Delta_{\text{HFC1-HFC2}}^2 [J(2J_{ex} - \omega_E + \omega_N)] + \\
& \frac{2}{15} \left( \aleph_{\text{G1,HFC1}} - \aleph_{\text{G1,HFC2}} - \aleph_{\text{G2,HFC1}} + \aleph_{\text{G2,HFC2}} - \right. \\
& \left. \aleph_{\text{ZFS1,HFC1}} + \aleph_{\text{ZFS1,HFC2}} + \aleph_{\text{ZFS2,HFC1}} - \aleph_{\text{ZFS2,HFC2}} \right) [J(2J_{ex} - \omega_E)] + \dots
\end{aligned} \tag{S10}$$

where the  $\Delta_{\mathbf{A}}^2$  is a matrix corresponding to the second rank norm squared [50] that arises from the anisotropy of a tensor  $\mathbf{A}$ ;  $\aleph_{\mathbf{A},\mathbf{B}}$  is a matrix corresponding to the second-rank scalar products of the tensors  $\mathbf{A}$  and  $\mathbf{B}$ . It arises from anisotropies associated to the electron Zeeman interaction tensor  $\mathbf{G}$ , the zero-field splitting

tensor, ZFS and the inter-electron dipolar interaction tensor, DD of the triplet 1 and 2 respectively. The terms containing  $J(\omega_E)$  do not contribute to the DNP enhancement and are omitted for simplicity.

#### D. Effects of the kinetic rates and of the $J_{ex}$ on the DNP enhancement

The effect of the kinetics rates, as a function of the  $J_{ex}$  on a hypothetical pentacene dimer molecule that can fulfill the JDNP condition ( $J_{ex} \approx \omega_E = 263$  GHz) at a high magnet field (e.g. 9.4 T) is shown in Figure S3. The strongest DNP enhancement was observed at the condition  $J_{ex} \approx \omega_E = 263$  GHz.

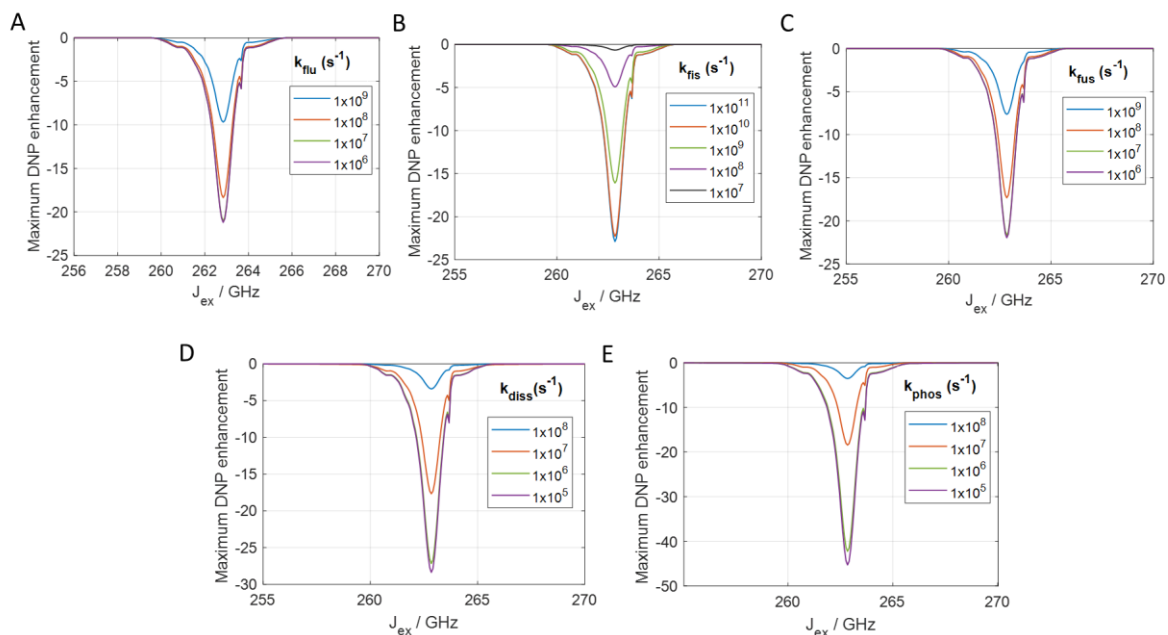


**Figure S3.** Effects of the kinetic rates and of the  $J_{ex}$  on the DNP enhancement: (A)  $k_{flu}$ , (B)  $k_{fis}$ , (C)  $k_{fus}$ , (D)  $k_{diss}$  and (E)  $k_{phos}$ . Simulations were performed at 9.4 T. While the kinetics rate is changed, the other rates and parameters were kept the same as those shown in Table 1.

### E. Effect of anisotropic $g$ -tensors on the self-relaxation rates and on the DNP enhancement:

As discussed previously, [20, 21] only rotations about the linker connecting the two monomeric units in a symmetric dimer (also in the case of triplet-pairs possessing nearly isotropic or axially symmetric  $g$ -tensors) can lead to a difference between the two anisotropic  $g$ - and ZFS-tensors. As discussed in the supporting information of [21], the  $\beta$  bending angle (about the linker connecting the two monomeric units) in long ( $\sim 38$  Å) linear linkers containing phenylene and acetylene units ranges between about  $0^\circ$  and  $\pm 40^\circ$ . Smaller displacements were expected for shorter linkers ( $\sim 14$  Å –  $20$  Å) as in the pentacene dimers considered for triplet-JDNP. Therefore, we calculated the DNP enhancements considering  $\beta$  and  $\beta'$  angles set equal to  $0^\circ$  and  $22^\circ$ , at 0.55 T, 9.4 T and 14.1 T, see Figure S4.

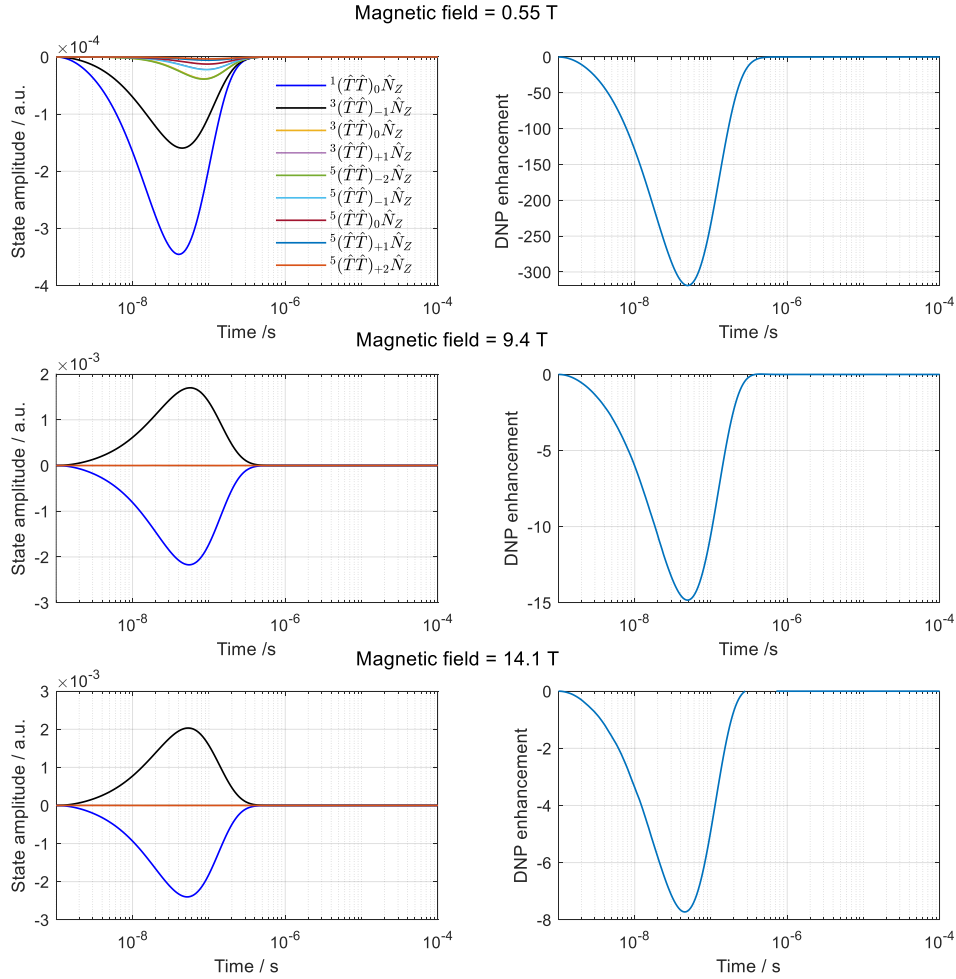


**Figure S4.** Time domain simulations performed at 0.55 T, 9.4 T and 14.1 T, showing the imbalance between the  $\alpha$  and  $\beta$  components of the triplet pair states (on the left) and the resulting DNP enhancement (on the right). The simulation parameters were set the same as those used in Figure 2 in the main text, but the  $\beta$  and  $\beta'$  angles were set to  $0^\circ$  and  $+22^\circ$ , while the angles  $\alpha$  ( $\alpha'$ ) and  $\gamma$  ( $\gamma'$ ) were set to zero.

In Figure S4, we observed a decrease of the DNP enhancement due to the decreased amplitude of  ${}^3(\hat{T}\hat{T})_{-1}\hat{N}_Z$  that changes sign at magnetic fields above 0 T. The magnitude of the self- and cross-relaxation rates of the states  ${}^3(\hat{T}\hat{T})_0$  and  ${}^3(\hat{T}\hat{T})_{-1}$  involved in the polarization process do not change in the case of

non-collinear  $g$ -tensors. However, we observed a change in the sign of the rate  $\Delta R_{\text{self},3/-1}$  that led to a change in  $\Delta R_{\text{self,tot}}$  (see Figure S5).

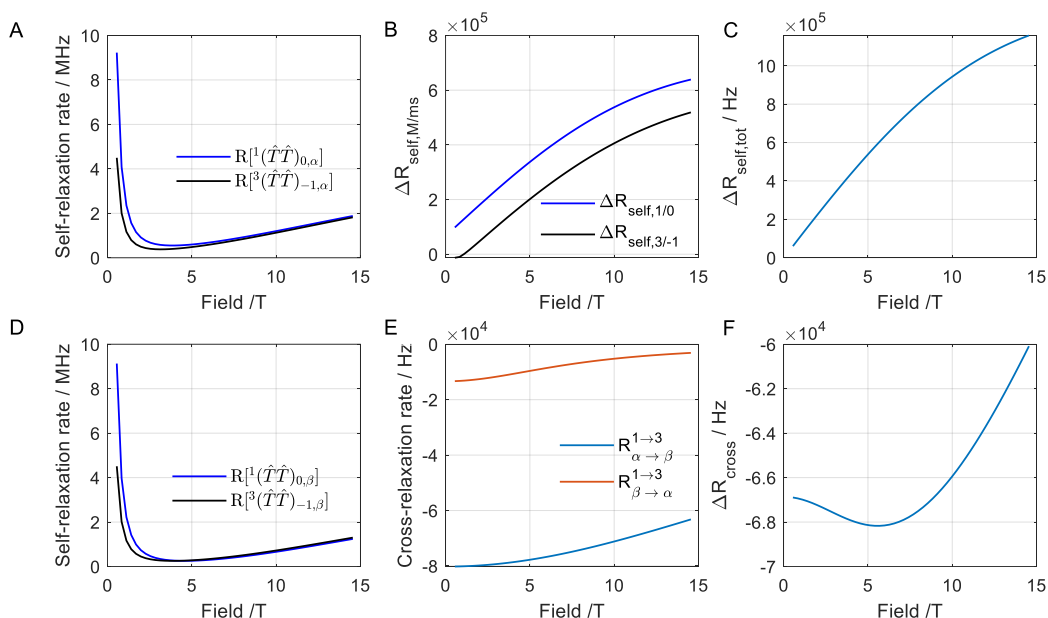


**Figure S5:** (A and D) Self-relaxation rates of the  $\alpha$  and  $\beta$  nuclear components of the triplet pair states  $^3(\hat{T}\hat{T})_0$  and  $^3(\hat{T}\hat{T})_{-1}$ , (B)  $\Delta R_{\text{self},M/ms}$  of the triplet pair states  $^3(\hat{T}\hat{T})_0$  and  $^3(\hat{T}\hat{T})_{-1}$ , (C) the difference in self-relaxation rates  $\Delta R_{\text{self,tot}}$ , (E) cross-relaxation rates  $R_{\alpha \rightarrow \beta}^{1 \rightarrow 3}$  and  $R_{\beta \rightarrow \alpha}^{1 \rightarrow 3}$ , (F) the difference in cross-relaxation rates  $\Delta R_{\text{cross}} = R_{\alpha \rightarrow \beta}^{1 \rightarrow 3} - R_{\beta \rightarrow \alpha}^{1 \rightarrow 3}$ , as a function of the magnetic field. The simulation parameters were set the same as those used in Figure 4 in the main text, but the  $\beta$  and  $\beta'$  angles were set to  $0^\circ$  and  $+22^\circ$ , while the angles  $\alpha$  ( $\alpha'$ ) and  $\gamma$  ( $\gamma'$ ) were set to zero.

The change of the sign of  $\Delta R_{\text{self},3/-1}$  led to a change in the sign and amplitude of  $^3(\hat{T}\hat{T})_{-1} \hat{N}_Z$  at magnetic fields above 0 T. It does not result in a change of the sign of the overall DNP enhancement, but just in a small reduction of it, see Figure S6.

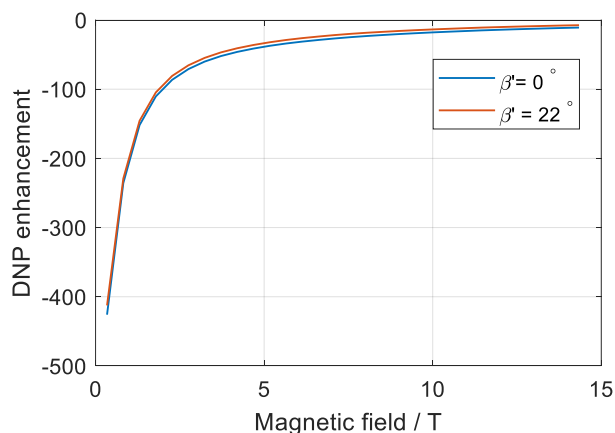


**Figure S6.** Comparison between the maximum enhancement obtained in the triplet-JDNP time domain simulations as a function of the magnetic field using the simulation parameters are given in Table 1 with the  $\beta$  and  $\beta'$  angles were

set to  $0^\circ$  and  $0^\circ$  (blue line) and to  $0^\circ$  and  $+22^\circ$  (red line), while the angles  $\alpha$  ( $\alpha'$ ) and  $\gamma$  ( $\gamma'$ ) were set to zero. The  $J_{\text{ex}}$  was set at the condition  $J_{\text{ex}} \approx \omega_{\text{E}}$ .

### References:

1. Blicharski, J., *Nuclear magnetic relaxation by anisotropy of the chemical shift*. Z Naturforsch Pt A, 1972. **27**: p. 1456-1458.
2. Concilio, M.G., I. Kuprov, and L. Frydman, *J-Driven dynamic nuclear polarization for sensitizing high field solution state NMR*. Physical Chemistry Chemical Physics, 2022. **24**(4): p. 2118-2125.
3. Concilio, M.G. and L. Frydman, *Steady state effects introduced by local relaxation modes on J-driven DNP-enhanced NMR*. Journal of Magnetic Resonance, 2023. **355**.